Angle-Resolved Desorption and Removal of Surface Nitrogen in DeNOx

Tatsuo Matsushima*
Catalysis Research Center, Hokkaido University, Sapporo 001-0021, Japan
e-mail: tatmatsu@mbr.nifty.com

Anton Kokalj
Department of Physical and Organic Chemistry, Jožef Stefan Institute, Jamova 39, 1000 Ljubljana, Slovenia
e-mail: tone.kokalj@ijs.si

Abstract

This paper reports on recent progress with angle-resolved desorption leading to structure-sensitive desorption dynamics. The sensitivity is exemplified in NO and N_2O reduction on Pd and Rh surfaces. The energy partitioning in the repulsive desorption of hyper-thermal products into their rotational and translational modes is an indispensable concept to examine the structure of a reaction site from desorbing molecules because it connects the structure of a transition state with each energy of desorbed products. The extent of the energy partitioning will be derived from the desorption-angle dependences of both the rotational and translational energies at each vibrational state. Such energy analysis has never been completed for any thermal reactive desorption. A new type of measurement is thus proposed. Additionally, we discuss the inadequate use of *the detailed balance principle* in desorption dynamics, which has prevented desorption dynamics from being sensitive to surface structures.

Key words: Spatial distribution, Transition state, Energy partitioning, NO reduction, N_2 desorption, Intermediate N_2O

High lights
1. Energy partitioning (EP) at desorption is connected with transition state structures.
2. Inclination of a transition state controls EP into rotational and translational modes.
3. Site sensitive desorption dynamics requires angle-resolved work of all product energies.
4. Use of detailed balance principle in desorption dynamics leads to wrong physics.

1. Introduction

This review delivers a brief history of how the desorption dynamics of hyper-thermal products has become sensitive toward surface structures as exemplified in the studies of N_2 desorption in NO reduction on Pd and Rh surfaces (best deNOx catalysts). A full review of deNOx catalysis is out of the scope of this paper since many reviews have already been published for the subject [1-5]. The structural analysis of a surface site is now nearly enabled from the desorption dynamics of hyperthermal products. Such a dynamical approach to the surface site was first tried with the spatial distribution of hyper-thermal products [6,7]. In last 10 years, the desorption angle dependence of the internal energy of desorbing product CO_2 has been successfully analyzed [8]. Furthermore, the peculiar off-normal N_2 desorption has been theoretically and experimentally analyzed [9-16]. The N_2 desorption has become a model probe for desorption dynamics. These results have opened an avenue to desorption dynamics sensitive to surface structures and then provided a stage suitable to propose new desorption measurements in the next generation. Our former reviews [17,18] just summarized angle-resolved desorption (ARD) experiments for CO oxidation and NO reduction. Now it is clear that the product flux and both the translational and internal energies must be analyzed as functions of both the desorption angle (polar angle, θ, with respect to surface normal (Fig. 1)) and the azimuth angle because the energy partitioning (EP) into translational and rotational modes of emitted products affects both the spatial and energy distributions [8,9]. This EP connects product energies with the structures of a transition state (TS) just like gas-phase reaction dynamics [9,19]. No such energy analysis has ever been completed for any thermal reactive desorption. Thus, a new set of angle-resolved (AR) desorption measurements is proposed in Section 5. The desorption-angle dependence of EP is required for the structure analysis of the surface site including a TS. The lack of this angle dependence has long been masked by the inadequate use of the detailed balance principle (DBP) as explained in Section 6 [9,20,21].

In general, a chemical reaction must be characterized with respect to not only chemical kinetics (concerned with reaction rates) but also reaction dynamics (dealing with energy flows) because material conversions are always accompanied with energy repartitioning [14,19]. In other words, chemical kinetics hardly describes the whole story of any reactive desorption on a metal surface. However, the mechanisms of chemical reactions on metal surfaces have long been examined from the viewpoints of chemical kinetics. The resultant mechanisms are frequently short-lived because chemical kinetics describes the reaction rate in a phenomenological way as a function of the reactant coverage and surface temperature. Such chemical kinetics still continues to be used in the field of chemical engineering, solid catalysis, and electrochemistry. In the past, surface reaction kinetics had essential problems in describing the non-uniform reactivity of surface species with varying coverage. With the development of computers, the interactions between adsorbed species, as well as their movements, came to be handled

by Monte Carlo simulations on lattice gas models [22]. However, the passive status of surface chemical kinetics remains invariant due to the absence of the description of energy flows into different modes during reaction events.

On the other hand, studies concerned with the dynamics of desorption processes were few before the pioneer work by Willigen in 1968 [23], probably because, before the 1970s, it was widely believed that the energy flow from surface species to a metal was completed in the order of several femtoseconds [24], and then the analysis of the energy partitioning during desorption was impossible. Thus, the studies of surface reactions had shifted too much to chemical kinetics. Unfortunately, the understanding of reactive desorption dynamics has not been significantly improved, even after hyper-thermal products were confirmed in several desorption systems [25]. Indeed, the relaxation time of vibrationally excited admolecules is in the order of a picosecond on metal surfaces, as experimentally confirmed in the early 1990s [26]. This means that a desorption process has a chance to be studied at a dynamical level when products are emitted before relaxation, however, surface processes before desorption are hardly studied at a dynamical level because of the difficulties of energy analysis of nascent products on a surface. The dynamics of the combinative desorption of H(a), D(a), or N(a) on metal surfaces has been examined by means of state-resolved population analysis of desorbed H_2, D_2, or N_2 by using resonance-enhanced multi-photon ionization time-of-flight (REMPI-TOF) [27,28] or laser-induced fluorescence (LIF) [29]. Dynamical behavior of their reverse processes (dissociative adsorption) has also been studied by means of seeded molecular beams (MBs) [28,30]. Our understanding of product desorption dynamics is, however, still far from that of gas-phase reactions [31].

In published studies of desorption dynamics, structural information of a surface site including a TS or intermediates is scarcely provided in contrast to similar issues routinely surveyed in gas-phase reactions. This lack of structural information is one of the reasons that dynamic studies have not become powerful enough to characterize surface reactions. It should be noted that most of the analyses of the internal energies of desorbing products have been performed in non-AR fashions [27,28] in which their independence of the desorption angle (or no anisotropy) is tacitly assumed, making desorption dynamics insensitive to surface structures. An anisotropy related to the site structure was first found in the spatial distribution of product CO_2 desorption in 1989 (Fig. 2) [17,32]. Indeed, in 2008, both the translational and rotational energies of product CO_2 have been confirmed to be coupled with each other and to depend on both desorption and azimuth angles [8]. The anisotropic distributions of these quantities provide the information of surface structures. Thus, AR measurements for both translational and internal energies are essential to obtain surface structural information from desorbing products. It is fortunate that remarkable anisotropic distributions have been found in desorbing product N_2 on the best deNOx catalyst surfaces (Fig.1) [18,33]. In the near future, we will have a suitable desorption model to deliver the angle dependences of translational and rotational energies, confirming EP in quantitative ways. This new desorption dynamics will be useful to examine the results from DFT calculations concerned with TS structures [30,34,35].

2. Priority of Desorption Dynamics

Generally, repulsive desorption is likely to be localized around a definite site because it is completed within a very short interval (in the order of a vibrational period) on a repulsive part of the potential energy surface (PES). Therefore, the structure of a desorption site can be analyzed in dynamical ways. On the other hand, it is difficult to analyze the structure of an adsorption site in similar ways. The interaction of incident species with a surface is initiated on every part of the surface, and its adsorption is unlikely to be completed near its impact place, since large amounts of energy are released during adsorption; then the resultant adspecies is mobile until it is stabilized on a final surface location.

2. 1. Direct Approach to a Desorption Site

A reaction site on a metal catalyst was in early periods simply speculated as an "active center" through chemical modifications affecting the product formation rate as well as its selectivity [36]. After the development of ultra-high vacuum techniques to keep a surface clean, the site has been identified or analyzed by means of combined methods of kinetic measurements with surface-sensitive techniques such as surface vibrational spectroscopy, X-ray photo-electron or absorption spectroscopy, diffraction methods, and scanning microscopy [37-44]. These modern methods provide structural information useful to construct a reaction site; however, their information is indirect (not always connected to the reaction site), because they are based on signals from non-reacting surface species. Even if surface spectroscopy can distinguish the signals of reacting species from those of non-reacting ones, the observed signals are still due to those before or after the related reaction event.

It should be noted that a surface desorption site is not just a point without size; it must have some spread. As exemplified in Section 4, several surface atoms work cooperatively to complete one desorption event. Thus, a site structure will be described by means of the PES of the product desorption system. Such a PES can be constructed, e.g., by means of density functional theory (DFT) calculations. On experimental sides, we need to provide definite knowledge of the respective desorption process to theoretical work, and also to confirm the structure of the calculated PES through the dynamical behavior of nascent products. Especially, the latter has not been possible because of the lack of methods to examine the structure of the desorption site including a TS. In fact, many TS structures have been predicted in DFT work, however, no confirmations have been reported based on experiments [34,35]. Thus, we need a

method to directly analyze the structures of sites or active intermediates through the reaction itself, namely from their products before energy dissipation. No such confirmation can be performed by either chemical kinetics or surface spectroscopy. The importance of these viewpoints will be recognized in the NO reduction studies described in Section 4, where it is shown that the wrong reaction pathways of N_2 emission had long been accepted on both experimental and theoretical sides [12,13].

In gas-phase reactions, methods for approaching the PES have been established, i.e., information on the TS conformation is deduced from the spatial and energy distributions of emitted products before energy dissipation for various collision energies [45] or by femtosecond spectroscopy during molecular transformation [46]. The TS structure is mostly examined from the distributions of both translational and rotational energies at each vibrational state when the products are emitted through a repulsive potential energy surface [19]. These modes are simultaneously excited and then strongly coupled with each other, resulting in the EP into translational and rotational modes.

A similar EP may take place in repulsive desorption on a metal surface, however, its principle has not yet been quantitatively confirmed in thermal (reactive) desorption because of the lack of observed desorption-angle dependences of the rotational and translational energies of hyper-thermal products at each vibrational state. Indeed, the internal energies of desorbed products have been analyzed by means of REMPI, LIF, or infrared (IR) emission in non-AR fashions except for Yamanaka's AR-IR emission analysis [8]. These non-AR treatments have neglected the desorption-angle dependences of the flux and energy distributions. For reactive desorption on a metal surface, the relation of TS structures to EP into rotational and translational modes has been recognized in Yamanaka's AR-IR work with nascent product CO_2 in CO oxidation on Pd surfaces in 2008 [8]. His observations regarding angle-dependent rotational energy have opened an avenue toward the EP in repulsive desorption, leading to a new stage of structure-sensitive desorption dynamics. However, even in his AR-IR work, IR emission was still analyzed in a non-state-resolved way.

2. 2. Short-Lived Intermediates

Angle-resolved desorption (ARD) analysis, as it is surface-structure sensitive, is superior to other surface-sensitive methods for the detection of adsorbed intermediates with a short lifetime inaccessible to surface vibrational spectroscopy. For example, such conditions are met when the heat of adsorption (or the activation energy to decomposition or desorption) of the adspecies is below approximately 50 kJ/mol at surface temperature (T_S) of 500 K; in this case a surface residence time is estimated to be in the order of a nanosecond by assuming first-order desorption. Under high vacuum conditions (below 0.1 Pa), such species can hardly be detected with surface spectroscopy because their relative coverage is below 0.0001. In the course of a catalyzed reaction, their detection becomes more difficult because of the presence of other reactants with higher adsorption heat. Good examples are found in the physical

adsorption of small molecules. Their adsorption bond energies are often below 50 kJ/mol [47], hence their adsorption states can hardly be observed in spectroscopic ways above T_S=500 K under a high vacuum due to too short residence time. Indeed, it is clear that the respective time domain is available only via desorption dynamics and is inaccessible via surface spectroscopy. Such situations may take place when surface residence times are in the order of 10 nanoseconds or less. The time required for fast adsorption and/or decomposition may be in the order of picoseconds close to the relaxation time of vibrationally excited admolecules [26,48,49]. The priority of ARD in such cases is due to the reactive desorption dynamics directly identifying surface sites or active intermediates. Thus, ARD and surface spectroscopy are complementary to each other in repulsive product emission because the former surveys active species at the exit of reactive desorption, whereas the latter monitors species at the desorption entrance.

Active intermediates such as N_2O(a) or $(NO)_2$(a) on metal surfaces often have small either heats of adsorption or activation energies for decomposition. These adsorbed species can be observed only at low temperatures and pressures with surface spectroscopy[50-53]; such observations are not successful for N_2O(a) in the course of the catalyzed NO reduction above 450 K [15,54,55], although it plays an important role as adsorbed intermediates yielding product N_2 on the main pathway of NO reduction on Pd, Rh, or Ir surfaces [15,18]. $(NO)_2$ on Cu(110) or Ag(111) is converted into N_2O(a) and then to N_2(g) [52,53, 56-58]. This species has been observed on Pd(111) at elevated NO pressures around 4×10^4 Pa and room temperature [59]. The N_2O formation vis such a dimer is likely to take place at high pressures.

N_2O(a) has also been confirmed to form under temperature programmed desorption (TPD) conditions from N(a) and NO(a) on Pt(533), Pd(110), Pd(211), and Rh(111) [60-63]. However, the N_2 emission from the decomposition of intermediate N_2O(a) had not been accepted in NO reduction on Pd or Rh surfaces [1,64-66] for a long time after the earlier proposals [67-69]. This is due to the absence of both spectroscopic observations of N_2O(a) and direct evidence of N_2 emission from N_2O(a) in the course of the catalyzed reaction above 450 K [54,55,70]. In fact, only ARD can directly confirm the contribution of N_2O(a) decomposition by showing the peculiar spatial distribution of the final product N_2 [14,17,18]. Before the ARD analysis of the product N_2 at steady-state NO reduction [18], the lack of direct evidence of the N_2 emission from intermediate N_2O(a) had led to the wrong assumption that N_2O(a) is formed in NO reduction on Pd or Rh surfaces, but in a bypath not yielding N_2 [61-65]. Based on these insights provided by ARD analysis, the N_2O(a) is now accepted as the pivotal intermediate leading to the final product emission on the main deNOx pathway as described in Section 4.

3. Structure-Sensitive Desorption Dynamics

3. 1. Hyper-Thermal Products

Some chemical reactions on metal surfaces emit products before thermalization to the surface temperature. The emission of such hyper-thermal products was first reported with $H(a)+H(a)\rightarrow H_2(g)$ on metal surfaces in 1968 [23], and it was later confirmed in several combinative desorptions such as $CO(a)+O(a)\rightarrow CO_2(g)$, $C(a)+O(a)\rightarrow CO(g)$, $N(a)+N(a)\rightarrow N_2(g)$ and $CH_3(a)+H(a)\rightarrow CH_4(g)$ [17,25]. On the other hand, in dissociative desorption, only the decomposition of $N_2O(a)$ to $N_2(g)+O(a)$ was confirmed to emit hyper-thermal products [18]. Surprisingly, this decomposition emits fast N_2 in two-directional (off-normal) ways on Pd(110), Rh(110), and Ir(110) (Fig. 1). For such fast desorption, the nascentproduct molecule must be formed on a repulsive part of the PES of the desorption event; i.e., the product is formed more closely to the surface than its equilibrium adsorption position. In such instances, the desorption is completed in a time interval comparable to a vibrational period. The resultant desorption yields hyper-thermal (or energetic) products and is sharply collimated along the direction of the repulsive force, yielding the maximum flux position (collimation angle). The translational energy is also maximized at this angle. In such repulsive desorption, the hyper-thermal products may hold the structural information of the desorption site including a TS or intermediates emitting products even after leaving the surface [14,17,18]. The memory of this repulsive force is likely to be preserved in the physical quantities of each desorbing molecule in anisotropic ways. Each emitted product holds only a piece of surface-structural information, and the site (or intermediate) structure will be reconstructed by gathering these pieces over all of the desorption and azimuth angles. This approach is essentially the same as that in gaseous reaction dynamics to the PES [31,45,46]. Therefore, AR procedures are indispensable in the desorption measurements to obtain surface-structural information. In contrast, translational or internal energy measurements without AR procedures cannot provide any surface structure information [20,27,28,71-73]. In other words, it is difficult to obtain surface-structure information when no azimuth-angle dependence is found in the AR signals of desorbed molecules.

Traditionally, reactive desorption has been classified into two categories, i.e., Langmuir-Hinshelwood type and Eley-Rideal one. In the former, all adsorbed reactants are equilibrated with the surface temperature before desorption as described above. In the other, pre-adsorbed species are directly attacked by incident reactants from the gas-phase (including hot atoms or oriented molecules). In the latter case, the flux and energy of desorbed products must be examined in the same way as that above but at various fixed states of the incident reactants.

3. 2. Energy Partitioning

In repulsive desorption, the released energy is partitioned into the translational,

rotational, and vibrational modes of desorbed molecules as well as the surface phonon modes. The energy partitioning (EP) into the first two modes strongly affects the desorption-angle dependences of the product flux and energies because these modes are simultaneously excited in desorption and then are coupled with each other [8,9]. The rotational mode is likely to be excited when the TS inclines against the surface plane as explained below. A similar concept concerning the decomposition of bent TSs into their fragments is well-known for gas-phase reactions [19]. Namely, due to repulsive forces, operative from the counter product, the nascent fragment not only accelerates its velocity, but also starts to rotate due to a torque induced by the Pauli repulsion, which rapidly decreases with an increasing distance between the nascent and counter products. Thus, larger EP to the rotational mode yields lower translational energy. The apparent angular (velocity) and rotational energy distributions depend on the extent of this EP. In other words, the bent form of a TS can be examined from the emission angle dependence of the EP.

In the repulsive desorption on a metal surface, a similar mechanism may be operative; i.e., the extent of the EP into the rotational and translational modes depends on both the inclination of the TS against the site plane and the repulsive forces exerted from the desorption site and/or the counter product. Similar EP is observed in the scattering of hot N_2 on Ag(111) and Ni(111) surfaces [74-77]. There, the energy transferred into rotational modes depends on the angle of the inter-nuclear axis of the molecule against the surface normal. At standing or lying N_2 on the impact, the energy transferred to rotation is zero and rises to a maximum at an intermediate angle. A similar energy transfer is expected in repulsive desorption, as sketched for a simplified TS of CO_2 formation in Fig. 3(a), i.e., a standing TS or a lying one is translationally excited in desorption, whereas an inclined TS is rotationally and also translationally excited.

The inclination angle of a TS will be distributed around the most probable position, especially for the weak adsorption bonding where the bending motion easily occurs [78]. Thus, typical flux distributions are drawn in Fig. 3(b) for a simplified model involving only two characteristic components, i.e., excited rotational (with slow translation) and hot translational (with cooled rotation) components in normally directed repulsion. In the figure, the cosine distribution is assumed for the former rotational excitation and a $\cos^{10}\theta$ form is used for the latter translational excitation. The total flux ratio of the former to the latter is assumed to be unity. It is clear that the molecules desorbing along the surface normal have high translational and low rotational energies because of the predominant fast component, whereas the product emitting at large off-normal angles has lower translational and higher rotational energies. With an increasing desorption angle, the observed translational energy decreases and the apparent rotational energy increases, as observed with the product CO_2 in CO oxidation on Pd(111) [8]. The translational temperature will even go below the surface value when the repulsive forces are highly converted into the rotational mode. It is reminiscent of the slow H_2 molecules at large off-normal angles on Ni(111), in which the translational temperature goes down from about 1.5 times the surface value at the normally directed desorption to about 70 % of the surface temperature at desorption angles above 60° [25].

For experimental confirmations of the EP model, it is worthwhile to consider how the translational and rotational energies vary under different conditions. In this model, the sum of both energies should be fairly constant at a fixed vibrational level, thus being independent of the desorption angle, the rotational energy level, and the azimuth angle, provided that the EP into the surface phonon modes is not significant. For this confirmation, both energies must be evaluated simultaneously in AR-fashions; i.e., AR-TOF measurements of desorbed products are necessary at each rotational and definite vibrational state. On the other hand, when those energies are determined with frequently used non-AR-REMPI-TOF, this relation does not hold because the translational energy is overestimated at high J values (rotational quantum number) when the EP into the rotational mode is significant. In particular, the higher the rotational energy is, the more the apparent kinetic energy is overestimated. WithNamely, for a definite rotational level, indeed, the velocity of produced ions is widely distributed [27,28]. Under repulsive forces operative to desorbing products toward the surface normal direction, the resultant faster components (yielding sharper spatial distributions) are more collected than the slower ones (broader distributions) in non-AR-REMPI-TOF, where the detector (an ion collector) faces a sample surface from the vertical. Typical efficiency of the ion collector with an acceptance angle of ±20° [79] is drawn in Fig. 3(c) in which the product desorption is assumed to be collimated along the surface normal (no anisotropy), showing the distribution of a $\cos(\theta)$ or $\cos^{10}(\theta)$ form. The flux on the vertical axis in the figure is already integrated over azimuth angles at each desorption angle. It should be noted that the ion collector with an acceptance of ±20° can receive only about 12 % of the total flux for the cosine distribution, and ca. 50 % for a $\cos^{10}\theta$ form (Fig. 3(d)). The received ion acceptance does not exceed 32 % for desorption with a form broader than $\cos^{5}\theta$. Hence, a TOF curve with reduced slower components yields higher translational energy than that averaged over all desorption angles. This means that the product molecules at a definite rotation level moving along the normal direction (faster components) are more accepted by the collector than that of off-normal components (slower ones) with the same J value because the current non-AR-REMPI-TOF collects only the molecules desorbed within limited desorption angles around the normal direction. Typical examples will be discussed in Section 6-4.

3. 3. Anisotropy in Energy Partitioning

The anisotropic properties of emitted products are essential to obtain the information on surface structures through desorbed molecules. Remarkable anisotropy in the spatial distribution of hyper-thermal products as well as their translational energy was first observed with desorbed CO_2 in CO oxidation on Pd(110)(1×1) by means of AR-TPD-TOF (Fig. 2) [32,80]. The CO_2 distribution is sharp (a $\cos^{12}\theta$ form) on the normally directed plane along the [001] direction and broad (a $\cos^{2}\theta$ form) on the plane perpendicular to it. This anisotropic CO_2 distribution is also observed in a steady-state

NO+CO reaction [33]. With an increasing shift from the surface normal, the translational energy decreases more rapidly along the [001] direction than along the [1$\bar{1}$0] direction (Fig. 4) [80]. At higher coverage, the kinetic energy is increased, and the anisotropy in the energy remains. These anisotropies in the flux and translational energy were proposed to be due to the anisotropy of the restricted motion of a TS parallel to the surface plane, which originates from the anisotropic structures around the desorption site; i.e., the surface-parallel motion of the TS prevails along the narrow troughs or facets because of the flat (111) structure [81]. In this reaction, the product CO_2 is likely to form at or around the adsorption site of O(a) since the metal–O(a) bond is strong (i.e., this bond rupture is slowest) and CO(a) is highly mobile. The spatial distribution of the resultant CO_2 desorption may be affected by the local structure around the oxygen adsorption site.

Similar anisotropy is observed on Ir(110)(1×1) and Pt(110)(1×1) and also in off-normal emissions on Pt(110)(1×2), Ir(110)(1×2), Pt(113)(1×2), and Pt(112)=[(S)3(111)×(001)] [17]. These (1×2) reconstructed surfaces commonly provide narrow and inclined facets with a (111) structure on which reactive CO_2 desorption preferentially takes place. The CO_2 desorption sharply collimates in the direction close to the local facet normal. It shows broad distributions on the plane (passing the collimation position) along the narrow facets whereas the distribution becomes sharp on the plane perpendicular to it. Anisotropic motions of the TS were again invoked in the CO_2 desorption on a narrow facet to explain anisotropic distributions of the translational energy and flux. This model does not involve the contribution of the EP into rotational modes.

In 2008, Yamanaka reported remarkable anisotropy in the rotational energy of product CO_2 in CO oxidation on Pd(110) (Fig. 5) [8]. On Pd(110)(1×1), the rotational energy decreases rapidly with an increasing shift from the normal direction toward the [001] direction, whereas the value somewhat increases or remains almost invariant along the [1$\bar{1}$0] direction. Thus, both the energies and product CO_2 are emitted more on the normally directed plane along the [1$\bar{1}$0] direction.

Here, a new desorption model is required in which the anisotropies in both translational and rotational modes are simultaneously induced in a single desorption event. The above EP into translational and rotational modes is controlled by both the resultant repulsion and the inclination of the TS. Thus, the above anisotropies will be expected in both modes when the TS inclines in limited directions. An inclined form of the TS to CO_2 formation has been predicted in DFT work on Pt(111) [82]. On Pd(110)(1×1), the TS to CO_2 may incline somewhat toward either the [1$\bar{1}$0] direction or in the opposite direction on the normally directed plane along the [110] direction. In this case, the product CO_2 is emitted more onto this plane than onto that perpendicular to it. The flux distributions should be broader along the [1$\bar{1}$0] direction than along the [001] direction, since two somewhat (oppositely) inclined components overlap along the [1$\bar{1}$0] direction, and no repulsive forces are operative on the plane along the [001] direction. Eventually, the anisotropy of CO_2 desorption on Pd(110) is affected by not only the anisotropic motion of the TS parallel to the surface plane but also the anisotropic EP.

The rotational temperature on the plane along the [1$\bar{1}$0] direction may increase or remain invariant with the increasing desorption angle since the repulsion makes the inclined TS torque as well as accelerates its velocity. On the plane perpendicular to it, no excitations are expected in either mode; i.e., both the rotational and translational energies should decrease rapidly with an increasing shift from the normal direction, as actually observed. However, for quantitative confirmations of this EP model, angle-resolved TOF measurements are required at each rotational state to examine the relation of the rotational energy to the translational energy at each desorption angle and vibrational level. Such experiments are not available at present with the product CO_2, as explained in the next section. Nevertheless, these considerations strongly suggest that an approach to the structure of a TS becomes possible when the EP is quantitatively evaluated as a function of the desorption angle. In other words, the inclination of a TS will be examined from the angle dependence of EP, i.e., the velocity distribution of product molecules at each rotational state must be analyzed as a function of the desorption angle.

Generally, this EP is likely to shift to the translational modes in combinative desorption yielding iso-nuclear molecules such as N(a)+N(a) → N_2(g) and H(a)+H(a) → H_2(g), since their TS is likely to be parallel to the surface plane except for thermal drifts which result in small torque. Indeed, the observed rotational temperatures of desorbed products are often below the surface value even when both the vibrational and translational temperatures are much higher than the surface value [27-29,79]. On the other hand, the EP may shift more to the rotational modes in C(a)+O(a)→CO(g), N_2O(a) → N_2(g)+O(a), or CO(a)+O(a) → CO_2(g), since the inclined TS forms are likely.

3. 4. Characteristics of the structure-sensitive desorption systems

For further developments of ARD as structure-sensitive desorption dynamics (SSDD), the EP into rotational and translational modes must be quantitatively evaluated at various desorption and azimuth angles. For such an analysis, the emitted hyper-thermal products must be examined using a method that combines the performance of desorption-angle resolved + state selective + time of flight (TOF) techniques. State selection can be mostly performed by REMPI. The resultant ions can be transferred into the subsequent TOF measurements. However, AR-REMPI-TOF measurements have not yet been successful for thermal reactive desorption, although they are popular in gas-phase reactions or electron- (or photon-) stimulated desorption on metal surfaces. There have been difficulties for thermal desorption. First, the product signals become extremely small after AR procedures. Second, no desorption systems have been properly selected for this purpose. Third, the necessity of AR analysis of the internal energy has long been masked by the inadequate use of DBP, as explained in detail in Section 6.

The first point will be improved by inserting a collimator (with two slits and

differential pumping [83]) in the space between the ionization point of REMPI and a sample surface [9]. The related technical problems will be discussed in Section 5. The second subject is important to proceed to the next stage of SSDD, because no further progress is expected with the current probe desorption of H(a)+H(a)→H_2(g) and CO(a)+O(a)→CO_2(g), as explained below. Indeed, we still do not have an ideal model system providing the desorption-angle dependence of each physical quantity of hyper-thermal products. Here, we consider how to select desorption systems suitable to exemplify the necessity of the concept of EP toward SSDD. A desirable desorption process should yield the following characteristics: (i) desorbing products with anisotropic distributions of their physical quantities; (ii) product molecules that can be state-selectively detected. This selection is performed by REMPI mostly before the TOF setup; and (iii) desorbing products with measurable EP into both rotational and translational modes.

According to these criteria, the selection of the combinative desorption of H(a) into H_2(g) over copper surfaces has been unfortunate. This desorption does not satisfy items (i) and (iii). The spatial distribution of desorbed H_2 is isotropic and the EP is largely shifted to the translational mode. Of course, we would be able to examine the orientation of the TS against the surface plane through the desorption-angle dependences of the rotational and translational energies even on a flat surface. However, no structural information on desorption sites can be derived from desorbing H_2 (or D_2), since their physical quantities (flux and kinetic energy) are isotropic over the surface plane [6,7]; i.e., the surface will behave as if it is structureless. Actually, such isotropic desorption is also found with CO_2 on Pd(111) and Pd(100) [84,85]. The product CO_2 does not resolve item (ii). CO_2 can be ionized via REMPI, but its state selectivity is very poor [86].

All three items (i-iii) will be resolved with the product N_2 from either the associative desorption of N(a)+N(a)→N_2(g) on Pd(110) and Ir(110) or the decomposition of N_2O(a)→N_2(g)+O(a) on Pd(110), Rh(110), Rh(100), or Ir(110). Desorbed N_2 itself has frequently been analyzed via REMPI-TOF in non-AR fashions [28,73]. In the former associative process, the N_2 desorption is collimated along the surface normal, and its distribution is anisotropic as described above. This desorption is found in a steady-state NO+H_2 (or CO) reaction on the non-reconstructed (1×1) form of Pd(110) [33], Rh(110) [87], and Ir(110) [15] at relatively high surface temperatures. The other N_2 emission is peculiar, being two-directional on the normally directed plane along the [001] direction (or four-directional on Rh(100) along both the [001] and [010] directions). The desorption on Rh(110) or Pd(110) will be a good candidate because of the high product yield.

No contributions of the energy partitioning into vibrational modes of desorbed products are considered in the above criteria, although hyper-thermal products often involve vibrationally excited molecules [27,28,73]. Experimentally, the relation between rotational and translational modes can be examined individually at each vibrational state because the energy required to excite a vibrational state is much larger than that for a rotational state.

4. N_2 emission in NO reduction

The product N_2 emission has widely been studied over many years due to the final process of catalytic deNOx treatments and also the reverse process of the rate-determining step of ammonia synthesis [1,64,65,88,89]. The mechanism of catalytic NO reduction has been at last established by means of ARD analysis of both steady-state NO and N_2O reduction in the presence of CO (or H_2) on Pd(110), stepped Pd(211)=(S)[3(111)×(001)], Rh(100), Rh(110) and Ir(110), as well as AR-TPD of NO or N_2O-covered surfaces [12-15,18,33].

Two N_2 emission channels have long been considered in NO reduction on Rh and Pd surfaces. One is the well-known combinative desorption of N(a) as N(a)+N(a) → N_2(g) prevailing at high surface temperatures. The other process works at temperatures below roughly 600 K as N(a)+NO(a) → N_2O(a) → N_2(g)+O(a). The participation of NO(a) and N(a) in this pathway has been derived from the kinetic analysis of N_2 production in transient procedures including TPD and also a steady state NO+CO reaction on Rh or Pd surfaces [67,68,90]. The role of N_2O(a) has long been debated before ARD analysis. Although the chemical kinetics of the NO reduction suggested the presence of intermediate N_2O(a), neither direct evidences of its decomposition to N_2 nor spectroscopic signals due to N_2O(a) were found in the course of the catalyzed reaction above approximately 450 K [54,55,70]. Therefore, the N_2 emission from the intermediate N_2O(a) was not accepted in NO reduction on these deNOx catalysts for a long time after the earlier proposals in 1978 [67,68]. In most of the review papers concerned with deNOx catalysis, the byproduct N_2O was considered to be formed in a bypath not yielding N_2 [1,64-66,91].

More than one year after the report of AR-TPD-TOF work providing the ample evidence of intermediate N_2O(a) emitting N_2(g) on Pd(110) [92], Zaera's group has argued the first identification of intermediate N_2O(a) in a steady-state NO+CO reaction on Rh(111) at 480 K from their observations of "exclusive" formation of $^{14}N^{15}N$ when the reactants of ^{14}NO + CO were quickly switched to a mixture of ^{15}NO and CO while $^{14}N_2$, $^{14}N^{15}N$ and $^{15}N_2$ products were simultaneously monitored [93]. Referring to their kinetic (Monte Carlo) simulations based on a lattice gas model [94,95], they argued that the $^{14}N^{15}N$ was due to the decomposition of ^{14}N-^{15}NO like complex formed from ^{14}N(pre-deposited)+ ^{15}NO(post-dosed), although $^{15}N_2$(g) was also significantly observed. These kinetic results are not enough to conclude that $^{14}N^{15}N$ comes from the short-lived N_2O(a). Rather, these isotopic compositions of desorbed N_2 should be explained by considering non-uniform reactivity of pre-adsorbed N(a) and post-deposited one in the combinative desorption as N(a)+N(a)→N_2(g). The reason is as follows. (1) the combinative desorption of N(a)+N(a) →N_2(g) is already significant at 480 K on Rh(111) [96]. (2) Belton has already reported that the nascent product N_2O(a) is merely desorbed as N_2O without decomposition to N_2+O(a) when the co-adlayer of

N(a)+NO(a) on Rh(111) is heated [61]. Similar nascent $^{14}N^{15}NO$ desorption without decomposition has been reproduced on Rh(111) with N(a)+NO(a) in Kondoh's group [93] although they proposed the NO dimer mechanism for N_2O formation as described in next Section [98]. (3) no separation of the product N_2 from the N-NO complex was successful from the N_2 from the combination of N(a)+N(a). (4) N_2O is molecularly adsorbed on Rh(111) around 100 K and desorbed in the subsequent heating without decomposition. Bowker suggested from his molecular beam work in a wide range of temperature that the small dissociation probably of incident N_2O on Rh(111) is due to adsorption on structure defects [99].

At elevated reactant pressures, isocyanate (-NCO) has been an intermediate candidate for a long time in the reaction of CO+NO on noble metals supported on oxides [100,101]. This species is observed in a steady-state NO+CO reaction even on Pd(111) by vibrational spectroscopy [54,102]. However, the pathway from this species to the final product N_2 is unclear. It might be just a spectator.

4.1. Intermediate N_2O(a) yields N_2

The role of the byproduct N_2O was unclear before the ARD analysis of the steady-state reduction of both NO and N_2O [14,18]. It is now accepted that the intermediate N_2O(a) yields the N_2 on the main reaction pathway of NO reduction; i.e., this intermediate either decomposes emitting N_2(g) in off-normal ways or desorbs as N_2O(g) without decomposition. Its branching strongly depends on the experimental conditions, such as the kind of metal, the surface structure, the amounts of co-adsorbates and the surface temperature [18]. It should be noted that the heat of adsorption is only 35–50 kJ/mol, and the activation energy to decomposition is even smaller. Therefore, as described in Section 2.2, it is difficult to detect the signals due to N_2O(a) with surface vibrational spectroscopy in the course of the catalyzed NO reduction above about 450 K [54,55,70]. Only ARD analysis has confirmed the participation of this intermediate in N_2 formation through its peculiar spatial distribution.

At low temperatures, around 60-120 K, and high NO coverage, the formation of N_2O(a) via a dimer of NO(a) as $(NO)_2(a) \rightarrow N_2O(a)+O(a)$ has been first derived on Ag(111) and Cu(110) by using reflection absorption infrared spectroscopy (RAIRS) and near-edge X-ray absorption fine structure (NEXAFS) [52,53,56-58]. This intermediate N_2O(a) decomposes to N_2 + O(a). On Rh(111) below 350 K, N_2O(a) formation involves $(NO)_2$ dimers from the second adsorption layer [97,98]. N(a) and NO(a) in the first adsorption layer do not participate in the N_2O(a) formation at low temperatures, but at higher temperatures above 350 K, its formation from NO(a)+N(a) in the first adsorption layer has been confirmed by using isotope ^{15}N and fast NEXAFS. Recent IR work at elevated NO pressures (4×10^4 Pa), the dimer $(NO)_2$ has been confirmed on Pd(111) [103]. The pathway of $(NO)_2$(a) to N_2O(a) is accompanied with N(a) formation. This remaining N(a) is likely to react with one of neighboring NO(a) to yield N_2O(a), i.e., two N_2O molecules are likely to be produced simultaneously via different pathways. It

will be difficult to differentiate these pathways to N_2O at high pressures. However, the contribution originating from the $(NO)_2$ dimer is unlikely for the N_2O formation in the steady-state NO reduction above 450 K at low pressures, except for the surfaces with no ability of NO(a) dissociation [52].

In the literature, Tanaka *et al.* found the off-normal N_2 emission in the AR-TPD of NO-covered Pd(110) in 1991 [104,105]. The N_2 desorbed at around 490 K takes on a sharp off-normal distribution expressed by $\cos^{46}(\theta + 38°)$ toward the [001] axis. This finding was a turning point regarding these issues because this peculiar desorption has eventually been developed into a unique method able to separately determine the decomposition of intermediate N_2O(a) to N_2 in the course of catalyzed NO reduction. Using an isotope tracer, they confirmed that, on Pd(110) and stepped Pd(211), this off-normal N_2 comes from the reaction of NO(a) with N(a); i.e., the heating of a surface with ^{15}N(a) and ^{14}NO(a) results in the emission of $^{14}N^{15}N$ off normal and $^{15}N_2$ along the surface normal [62,63]. They proposed a desorption-mediated reaction, NO(a)+N(a) → N_2(g)+O(a), in which the product N_2 is formed by a reaction with the anisotropic collision of moving N(a) with NO(a) without passing the intermediate N_2O(a) [91,106]. Although a measurable amount of product N_2O is found in the temperature range of the off-normal N_2 emission, Tanaka *et al.* neglected the decomposition of intermediate N_2O(a) to N_2 without any explanation [92,107]. Indeed, at that time (in the 1990s), this reaction pathway, which does not involve the intermediate N_2O(a), was widely accepted at low temperatures in the field of deNOx catalysis as described above [1,64,65,91,105,106]. Furthermore, from the absence of such off-normal N_2 emission in subsequent cooling in the presence of H_2 and NO, they argued that this off-normal desorption channel was not involved in the catalyzed NO reduction [62,63,91]. However, this argument does not take into account that, in general, there are differences in the reaction rate at a definite temperature between heating and cooling during temperature-programmed reaction (TPR) procedures because of the non-steady-state conditions in both directions. These different rates are caused both by the differences in the surface composition including adsorbates between the two procedures, and by the presence of a significant activation energy of the desorption process, yielding a product desorption rate depending on a heating or cooling schedule. In fact, the above differences in the N_2 distribution completely disappear in the heating and cooling cycle under the well-controlled steady-state conditions (Fig. 6) [13]. The off-normal N_2 emission process is an important part of the catalyzed NO reduction.

In the literature concerning the mechanistic studies of NO reduction on Rh surfaces, the conversion rate of gaseous N_2O to N_2 was frequently compared with that of NO to N_2 [69,108,109]. The former N_2O to N_2 reduction is much slower than the latter NO to N_2 one at low temperatures, since the surface is highly covered by NO(a), CO(a) or N(a), and then the adsorption rate of gaseous N_2O is reduced because of the small heat of adsorption [110]. However, in the NO reduction, the intermediate N_2O(a) is formed from NO(a) and N(a) on the surface without its adsorption process and then quickly either decomposes to N_2 or desorbs without decomposition. No conclusive mechanism

was derived for the N_2 emission from these comparisons because of the different pathways.

4. 2. Off-Normal Emission Pathway

The above desorption-mediated reaction mechanism has been repeatedly excluded by reproducing the identical off-normal N_2 emission in the AR-TPD-TOF of N_2O-covered Pd(110) or Rh(110) in the absence of NO(a) and N(a) since 1999 [18,92,111-113]; i.e., N_2O(a) decomposes below 200 K yielding off-normal N_2. The off-normal N_2 desorption shifts to around 490 K when TPD procedures start from NO-covered Pd(110) because the peak temperature is mostly controlled by the slow dissociation of NO(a), while the decomposition of N_2O(a) is fast. Thus both NO(a) and N(a) are required to form N_2O(a); however, the state of neither NO(a) nor N(a) affects the off-normal N_2 emission.

In NO reduction at relatively low temperatures, N_2 originates from the N_2O(a) intermediate, which forms from NO(a) and N(a). The participation of short-lived intermediate N_2O(a) in the N_2 formation can be directly confirmed through the reactive desorption itself because of the peculiar spatial and velocity distributions (i.e., hyper-thermal, two-directional, and concentrated on the plane along the [001] direction) [18,92,111,112]. In other words, only ARD analysis can confirm the reaction of intermediate N_2O(a) to N_2 in the course of catalyzed NO reduction. This peculiar desorption is also found in a steady-state NO + CO (or H_2) reaction on Ir(110) and Rh(100) (four-directional on this surface) below about 600 K, indicating that the intermediate N_2O(a) causes the off-normal N_2 desorption [18,113]. All these imply that the N_2O decomposition is the final process of N_2 emission on the main pathway of deNOx processes on Pd, Rh and Ir surfaces.

In a steady-state N_2O+CO (or H_2) reaction on Pd(110), Rh(110), or Ir(110), the product N_2 is only emitted in two-directional (off-normal) ways on the normally directed plane along the [001] direction. These off-normalN_2 emissions are observed at temperatures of 300-880 K when H_2 is used as a reducer [113]. Of course, such off-normal N_2 desorption is reproduced in the AR-TPD of N_2O-covered Rh(110), Rh(100), or Ir(110) below 250 K [18]. Among these surfaces, the N_2 yield is the highest on Rh(110).

At high temperatures above approximately 550 K, the contribution of the N_2 emission through N(a)+N(a)→N_2(g) increases in the NO reduction on Pd(110), Pd(211), Rh(100), or Ir(110) because of the reduced amount of NO(a) and the high activation energy of the combination process (Fig. 7) [113-115]. The N_2 desorption through this process is collimated along the surface normal on Pd(110)(1×1) and Ir(110)(1×1), showing a sharp angular distribution along the [001] direction and a broader one on the plane perpendicular to it [15,18].

4. 3. Off-Normal Emission Mechanism

Recent studies of N_2O(a) decomposition have provided new developments in SSDD and advanced analysis of the catalyzed NO reduction on Pd, Rh and Ir surfaces. Furthermore, DFT-GGA work has been essential in understanding the off-normal N_2 emission. This section summarizes how this peculiar phenomenon has been analyzed.

According to Tanaka's desorption-mediated mechanism, the anisotropic collision of moving N(a) with NO(a) leads to off-normal N_2 emission [91,106]. Their mechanism, however, does not take into account the energy balance. Namely, the kinetic energy of the off-normal N_2 reaches around 45 kJ/mol at the collimation position [92,111], whereas the thermal energy of desorbing NO(a) or moving N(a) is much lower, around 8 kJ/mol at 500 K. The latter energy is therefore insufficient to yield the off-normal N_2 emission, hence the energy source causing the off-normal N_2 desorption must be due to the formation of either an O–Pd or N–N bond in the NO(a)+N(a)→N_2(g)+O(a) process (without N_2O(a)). As for the direction of desorbed N_2, Tanaka *et al.* have argued that the orientation of the reaction coordinate of the above process is responsible for the off-normal N_2 emission [62,91]. However, they have never explained their *reaction coordinate* although the process involves several surface atoms and two reactants: thus there are many variables leading to the N_2 desorption that cannot be differentiated without theoretical considerations [62,63,91,106].

The swing desorption of nascent N_2 was proposed in 2002 by Kokalj within the framework of DFT-GGA [112,115] as a mechanism of its off-normal N_2emission in the decomposition of bent N_2O (bonded via terminal N and O atoms) oriented in the [001] direction on fcc(110) surfaces. The model has recently been elaborated for N_2O(a) decomposition on Pd(110) and stepped Pd(211)=[(S)3(111)×(001)] [12,13]. In this mechanism, the released energy largely flows from the counter product O(a) to the nascent N_2; i.e., the energy used for acceleration of nascent N_2 mostly originates from the metal-oxygen bond formation (above 450 kJ/mol) [116]. Kokalj predicted two adsorption forms of N_2O on Pd(110) as shown in Fig. 8(a). A standing form bonds through the terminal nitrogen to the surface atom (S-type) and a lying form is oriented along the [001] direction (L-type) [115,117]. The conversion between these two forms is facile because of the flat PES in between. The L-type was later confirmed by scanning tunneling microscopy at 14 K [118] because of the small heat of adsorption yielding a high mobility except for very low temperatures. The co-adsorption of the two forms was also confirmed with NEXAFS at 60 K [119].

The L-type is apt to dissociate since the terminal oxygen is easily deposited on the surface [117]. This species is bound to the surface via terminal N and O atoms and is considerably bent (Fig. 8(b)(i)) because of the charge-back donation from the metal. The N_2 emission starts by breaking the N–O bond in N_2O(a). Immediately after this bond rupture, repulsive forces are operative between the nascent N_2 and the counter-product O(a) (Fig. 8(b)(ii)). At this moment, the N–Pd bond is not yet broken, i.e., the interaction of the N_2 with Pd atoms is attractive. Then, the nascent N_2 swings over the bonding metal atom passing the most stable standing form (Fig. 8(b)(iii)) to an inclined position on the opposite side and experiences repulsive forces from the surface (Fig.

8(b)(iv)). The sequential break of the terminal N–metal bond lets the nascent N_2 fragment finally leave the surface (Fig. 8(b)(iv)).

According to DFT-GGA calculations, the N_2–surface bond is the weakest when the molecular axis is at around 35° off normal during the N_2-swing on Pd(110) and Rh(110) [13]. This indicates the enhanced possibility of the off-normal desorption when the N_2 fragment swings toward this angle. The resultant collimation angle will shift more off normal when the repulsive forces from the counter oxygen are strong enough. This model predicts larger off-normal angles with stronger repulsive forces from the counter-oxygen atom. Thus, the collimation angle on Pd(110) may be smaller than that on Rh(110) or Rh(100) because the repulsion is expected to be stronger on rhodium than that on palladium, considering smaller work functions [120] and smaller lattice constants on rhodium; i.e., more polarized oxygen at shorter distances is formed on Rh surfaces.

According to this model, the collimation angle on Ir(110) will be between the above two metals. Three-dimensional (3D) analysis of the product N_2 desorption has recently been completed in steady-state N_2O reduction on a (110)(1×1) form of Pd, Rh, and Ir. The off-normal N_2 emission is commonly maximized on the normally directed plane along the [001] direction on Pd(110) [33], Rh(110) [16], and Ir(110) [15]. The respective N_2 distributions at this azimuth are in a form of $\cos^n(\theta \pm \theta_0)$ with θ_0=41-51° and n=20-50 on Pd(110), θ_0=46-58° and n=8-12 on Ir(110), and θ_0=60-70° and n=8-10 on Rh(110), where θ_0 is the collimation angle and n is the sharpness parameter. The sequence of the collimation angle, Pd(110) < Ir(110) < Rh(110), is consistent with the above intuitive prediction. These parameters are fairly insensitive to the surface temperature.

4. 4. Potential Energy Surface of Swing Desorption

The above considerations of the product emission in deNOx pathways have enabled the construction of the PES of the swing motion of nascent N_2. The calculated PES will be useful to survey which orientation of the fragment reduces the adsorption bonding below the critical value for desorption. Thus, the PES of a N_2O/Pd(110) system has been calculated during the swing motion by means of DFT-GGA. On this surface, the most stable (lying) N_2O form is adsorbed on the top site, whereas N_2O adsorbed at the bridge site is less stable [12,115,117]. The calculations, however, reveal that the energy of the transition state for the dissociation of top-bonded N_2O is higher than that for bridge-bonded N_2O. Top-bonded N_2O is likely to first diffuse to a nearby bridge site and to dissociate there, because the respective cumulative energy barrier (for both diffusion to a bridge site and dissociation there) is smaller than the dissociation barrier at the top site. This is due to the movements of the counter-product oxygen; i.e., at the bridge site, O bonds directly to the stable bridge site, whereas at the top site, the O fragment initially bonds to the top site and, only after the N−O bond is broken, diffuses to the stable bridge site. Immediately after the N−O bond is broken, the respective fragments

(O and N_2) individually bind to the surface and then experience large mutual repulsive forces. Due to these forces, the N_2 swings over the adsorption site to the opposite side.

In Fig. 9, the DFT-GGA calculated PESs are shown for the swinging of nascent N_2 over both the on-top and bridge sites (both for swinging along the [001] direction), where the minimum energy path (MEP) for the upright-N_2 → flat-N_2 transition on Pd(110) is shown for top- and bridge-bonded N_2. ΔE is defined as $\Delta E = E_{site} - E_{0site}$, where E_{0site} is the potential energy of the equilibrium upright N_2 adsorbed at the site, E_{site} is the energy of a given configuration at that site, and site is either the top or bridge. For each point on the MEP curves, the corresponding structures are shown on the pertinent filmstrip (upper (lower) filmstrip corresponds to the bridge (top) site). The inset shows the definition of the N−N−metal bend angle t_1, the tilt angle t_2 between the N−metal bond and the surface normal, and the angle t_c between the surface normal and the axis linking the N_2 mass center with the adsorption site. For all but the first point on the MEP, the (t_1, t_2) angles are also stated.

The resultant PES for the swing motion is considerably more repulsive for the bridge site, whereas the adsorption bonding of N_2 is considerably stronger at the top site. The PES is repulsive enough to yield the desorption of N_2 only at the bridge site, where the barrier for the upright → horizontal transition is 0.21 eV larger than the adsorption energy magnitude of N_2. In contrast, at the top site, the barrier for the upright → horizontal transition of N_2 is 0.1 eV smaller than the N_2−metal bond strength, which implies that N_2 undergoes an upright → horizontal transition rather than desorption. It seems plausible that, at the bridge site, the N_2−metal bond is broken somewhere between the intersection of the MEP curve with the $|E_{ads}|$ line (lower bound) and the transition state (upper bound). The respective t_1 and t_2 angles are approximately 20° for the lower and 40° for the upper bound. If, instead of (t_1, t_2) angles, the angle between the surface normal and the axis linking the adsorption site with the center of the mass of N_2 (angle t_c, defined graphically in the inset of Fig. 9) is considered, then the respective t_c values are in a range from approximately 30° (lower bound) to 50° (upper bound). This range is consistent with the N_2 collimation angles of 40−51° that are actually observed on Pd(110).

This swing desorption model also explains the distribution of product N_2 from the decomposition of N_2O(a) on stepped Pd(211)=[(S)3(111)×(100)] (Fig. 10(a)). In the report of AR experiments, the N_2 desorption is sharply collimated at 25−31° off normal toward the step-down direction (defined in Fig. 10(b)) in the AR-TPD of either N_2O-covered [121] or NO-covered Pd(211) [13,63]. In the former, the desorption peaks at around 110 K and in the latter case of NO, it is maximized at around 510 K since their rate-determining steps are different from each other as observed on Pd(110). Nearly identical distributions of the off-normal N_2 emission are also observed in steady-state NO+D_2 and NO+CO reactions on Pd(211) below about 550 K (Fig. 6) [12,13]. In these NO reductions, of course, the decomposition of intermediate N_2O(a) emits the product N_2. According to the above swing model, a suitable pre-dissociation state of adsorbed N_2O should be oriented perpendicularly to the step-edge direction, such that the terminal oxygen atom can be deposited on step Pd atoms. On this stepped surface, N_2O

adsorbs in S-type form through the terminal nitrogen atom bonded to the step-edge (Fig. 10(b)) [12]. This adsorption form is, however, too far away to release the terminal oxygen atom onto the adjacent step-edge. Hence, the DFT-GGA calculations predicted that, in the course of dissociation, the N_2O first diffuses from step-edge to the central Pd row on the terrace and then tilts toward the nearest step in the step-up direction (Fig. 10(c)) and bends with the terminal O toward the bridge site at the step edge; as the bending increases the N–O bond concomitantly elongates and eventually breaks (Fig. 10(d)) [12,119]. A similar dissociation was first proposed on stepped Pt(211) by Burch [123]. After the N–O bond cleavage the nascent N_2 swings on the terrace toward the step-down direction due to repulsive forces from O(a) deposited on the step atoms (Fig. 10(e)). The DFT-GGA calculated PES for the respective N_2 swinging motion is shown in Fig. 11. Thus, the N_2 desorption collimates at 40-51° off normal from the terrace normal direction in a way similar to that on Pd(110), yielding an angle 21-32° off normal from the (211) surface normal because of the 19.5° inclination of the (111) facet (Fig. 10(a)). The NN–O dissociation followed by the swing desorption of the nascent N_2 fragment enhances the rotational and translational energies of emitted products. It should be noted that several metal atoms directly interact with the reactant N_2O(a), which dissociates and emits N_2, indicating a spread reaction site.

The swing desorption model therefore predicts a bidirectional inclined desorption of N_2 on fcc (110) surfaces on the plane along the [001] direction, whereas on fcc (211), it naturally predicts, in agreement with experimental observations, a unidirectional inclined desorption of N_2 in the plane along the $[1\bar{1}\bar{1}]$ direction, because N_2O can dissociate only when it bends with its O atom toward the upper step. The combination of fcc (110) and (211) examples thus provides a strong confirmation of the swing-desorption model.

The dissociation of N_2O(a) was frequently examined in several DFT-GGA studies on Rh(111), Rh(110), Pd(110), Ir(100), Pt(211), Pd(211), and Ni(755) [115,117,115-128], where the reaction was commonly treated as $N_2O(a) \rightarrow N_2(a)+O(a)$. These calculations evaluated the minimum-energy path of the N_2O(a) dissociation on the PES. Such static calculations are unable to describe the actual dynamics, because during the decomposition of N_2O(a), a large amount of energy is released, which ejects the N_2 from the surface; i.e., in AR-TPD experiments, product N_2 with high kinetic energy is emitted in the decomposition of N_2O(a) on Pd(110) [92,111], or hyper-thermal N_2 is observed even below the desorption temperature of N_2(a) on Rh(110) [129], indicating the formation of energetic N_2 directly from N_2O(a), i.e., the N_2 desorbs before being thermalized on the surface.

The above swing desorption model partitions the energy received from the repulsive force into the translational and rotational modes and then predicts that the velocity of N_2 is maximized at the collimation position and decreases with the increasing shift from it. On the other hand, the rotational energy is minimized at the collimation angle and increases with the increasing angle shift, keeping the sum of both rotational and translational energies constant. Thus, the desorption-angle dependences of the translational and rotational energies of the above N_2 will be useful for confirmation of

the EP model when both energies are simultaneously determined with AR-REMPI-TOF.

4. 5. Selectivity of NO Reduction

In the field of deNOx catalysis, one of the goals is to minimize the formation of harmful byproduct N_2O with elevated greenhouse effects [1,108,130-132]. The selectivity to N_2O at low temperatures has been considered to be controlled by either the disproportionation of NO(a)+N(a) toward N_2O and N_2 or the re-adsorption of emitted N_2O and its subsequent reduction to N_2. The former disproportionation was proposed in the kinetic analysis of transient N_2 formation in a high vacuum, as described above, and the latter readsorption/reduction came from TPR work at high reactant pressures (above 1×10^{-2} Pa) [1,69,70,108,125-127]. In these treatments, the decomposition of intermediate N_2O(a) (before desorption) toward N_2 has been omitted. At high temperatures, the combinative process of N(a)+N(a) contributes to the N_2 formation,

Keeping with such understanding, many modifications of catalyst surfaces, as well as different combinations of metals and supporting materials, were examined to suppress the yield of byproduct N_2O [1,130,133-139]. The reported selectivity of the NO + CO reaction to N_2O is in the order of Pd(111) > Pd(100) > Pd(110) [133-13135,140] or Rh(111) > Rh(100) > Rh(110) [136]. As this model neglects the decomposition of the intermediate N_2O(a), these orders were once explained as follows: “more open surfaces run the NO dissociation faster (at high NO coverage) and are more selective for N_2 because of higher N atom coverage” [135,136]. This does not explain the extent of N_2O formation itself. Furthermore, the reactivity of N(a) depends remarkably on the surface structure, i.e., the combinative desorption of N(a) on Rh(100) [113] is much slower than that on Rh(111) [96] or Rh(110) [87]. The above confirmation that the N_2O(a) intermediate plays an essential role in the main pathway to N_2 suggests new approaches toward innovative deNOx catalysts. Modifications of catalyst surfaces should be designed toward the state of N_2O(a) before desorption although the amount of N_2O(a) is too small for evaluation in the course of catalyzed NO reduction.

On Ag(111) and Cu(110), N_2O(a) is formed from $(NO)_2$(a) at high NO coverage. This pathway has not been confirmed to contribute to the N_2 emission in the catalytic NO reduction at working temperatures above approximately 450 K at low pressures, as explained in Section 4.1. As described above, recent vibrational spectroscopy work has confirmed the formation of adsorbed $(NO)_2$ dimer at high NO pressures [103]. The contribution to the N_2 formation through these dimers at high pressures will be a next research subject to be challenged. There, it is not easy to differentiate the N_2O formation pathways since the process of $(NO)_2\rightarrow N_2O(a)+N(a)$ may induce another N_2O formation as $N(a)+NO(a)\rightarrow N_2O(a)$ in the presence of surrounding NO(a). Desorption dynamics is not useful for the N_2O formation before N_2 desorption.

On flat as well as stepped surfaces of Pt, Pd, or Rh, N_2O is easily formed as $N(a)+NO(a) \rightarrow N_2O(a)$ as confirmed in TPD procedures of NO-covered surfaces when N(a) is deposited [60-63]. According to this mechanism the selectivity at low

temperatures is mostly controlled by branching of the intermediate N_2O(a) into decomposition and desorption. The extent of this branching strongly depends on the surface temperature, the kind of metal, its surface structure and the amounts of co-adsorbed species including N_2O(a) itself [17].

In general, the selectivity to N_2O must be smaller when the intermediate N_2O(a) easily dissociates; i.e., the dissociation tendency should be in the inverse order of the selectivity to N_2O. In fact, N_2O(a) desorbs without dissociation on Pt(111) [141], Ir(111) [142], Rh(111) [99], Ni(111) [143], and probably Pd(111) [144]; note that on these (111) surfaces the dissociation may proceed only on structural defects [99]. On the other hand, on open surfaces such as Pd(110), Ir(110) [145], and Rh(110) [17], N_2O(a) easily dissociates at around 100 K in the subsequent heating, thus emitting N_2. It also dissociates, to a small extent, below 100 K on Rh(100) [146] and Pd(211) [121]. No dissociation takes place on Pd(100) [113]. Furthermore, deposited O(a) modifies both the heat of adsorption of N_2O(a) and its activation energy to decomposition [18,129,147,148]. This makes the N_2 desorption spectra in the TPD of N_2O-covered surfaces complex [18,149,150]. Thus, the selectivity to N_2O is affected by many factors.

At high temperatures, the total selectivity toward N_2O is largely affected by increased contributions from the combination of N(a)+N(a) to N_2. This has been confirmed by ARD analysis since the N_2O(a) decomposition emits N_2 in off-normal ways, whereas the combinative desorption of N(a)+N(a) shows the normally directed desorption. On Pd(211) (Fig. 6), at higher temperatures the AR N_2 signal at -31° decreases rapidly, whereas the AI-N_2 signal decreases slowly. On Pd(110) (Fig. 7), the AR N_2 signal at 40° decreases above 550 K and that in the normal direction decreases more slowly above 650 K.

5. Developments of Structure-Sensitive Desorption Dynamics

Now it is clear how SSDD can be developed to an advanced stage. This will be performed by measuring all the energies of desorbed hyper-thermal products as well as their fluxes as functions of both the desorption and azimuth angles. No such measurements have ever been completed for any thermal reactive desorption because of the extremely small signals after AR procedures and the unsuitable selection of desorption systems as described in Section 3-4. New kinds of measurements are therefore required in the form of angle-resolved, state-specific and time-of-flight analysis. The new method must be able to evaluate the desorption-angle dependence of the EP into rotational and translational modes at fixed vibrational states. Such analysis is already popular for gas-phase reactions by means of velocity-selected crossed-MBs combined with AR-REMPI-TOF [31]. On metal surfaces, similar measurements have been performed in electron- (or photon-) stimulated desorption ion angular distribution (ESDIAD)-TOF by using short pulses of electron (or photon) beams [151,152] or in the scatterings of simple molecules, such as N_2 or H_2, by using short-pulsed MBs combined with REMPI-TOF [74-77,153]. In these experiments, no differential pumping is used in

front of a detector.

In the ESDIAD-TOF, emitted products are ionized near (several mm from) a sample surface with REMPI, and the resultant ions are detected on a position-sensitive screen in a time-resolved way. This will provide the AR-TOF of ions produced at each rotational state. Thermal reactive desorption cannot be examined in this way, since no such desorption pulses short enough for TOF measurements are provided. In the latter, the molecules scattered on a sample surface are ionized far (around 2 cm) from the surface, also with REMPI in an AR-way. There, in order to examine the desorption-angle dependence, the laser focus point (i.e., the ionization place) is transferred in the lobe of desorbed products on an arc around the cross point of the incident MB and the surface plane [76,153]. Referring to the timing of the MB pulses, the flight time of the molecules scattered on the surface is measured from the MB gate to the laser focus point. The observed time involves the flight time from the MB pulse gate to the surface and from the surface to the laser focus point + the surface residence time for product desorption. This method works only for simple scatterings since the observed flight time includes the surface residence time of reactant-product conversion. This TOF method is not applicable for reactive desorption because the surface residence time of product desorption is in a wide range up to the order of a millisecond or more, depending on the surface temperature and the activation energies for desorption of incident reactants and desorbed products [154]. TOF measurements are usually performed with a time resolution of a few microseconds. In order to avoid the ambiguity due to the surface residence time, the flight path for TOF must be set up only for the flight after product's leaving the sample surface. The above mobile laser focus method has recently improved by using two lasers and ion imaging techniques [155].

For AR-REMPI-TOF measurements of reactive desorption, the ionization place must be far from the sample surface, probably around 40 mm. This distance is important because it strongly affects both the signal intensity and the angle resolution, as well as the performance of differential pumping of the space between the scattering (reaction) chamber and the analyzer (ion collector). The signal intensity would be decreased by about three orders of magnitude as compared with that in non-AR fashion [156]. The performance of the angle-resolved procedures for thermally desorbed molecules has already been evaluated by Kobayashi and Tuzi [83]; i.e., at least two slits between the analyzer and scattering chambers (i.e., totally, three rooms) and a high pumping rate of the space between these slits are absolutely necessary. This collimator must be constructed between a sample surface and the ion collector. Thus, the velocity distribution of desorbing ionized products is determined from TOF measurements through a field free region. It will be important to construct a compact collimator and a good vacuum around the ion collector because of the highly sensitive REMPI method.

For desorption with symmetric (isotropic) distributions around the surface normal axis, the current non-AR REMPI-TOF can be converted into an AR-usage by constructing an ion collector with adjustable acceptance angles. As explained in Section 3-2, the acceptance of product ions yielded by REMPI is limited around the normal direction. AR-TOF at a fixed desorption angle may be numerically extracted from non-

AR-TOFs at different acceptance angles without large signal reduction due to AR-procedures. This simplified method is worthwhile to be examined for hydrogen desorption.

Reaction conditions in ARD work must be carefully considered. We can reproduce the hyper-thermal product desorption of $2H(a) \rightarrow H_2(g)$, $2N(a) \rightarrow N_2(g)$, or $N_2O(a) \rightarrow N_2(g) + O(a)$ on several metal surfaces, under either steady-state or non-steady-state conditions. Both conditions have their own advantages. Under steady-state conditions, the signals due to background gases become significant because of the presence of reactants at pressures (mostly) much higher than those of the products due to a small surface area of the sample crystal. This background value must be subtracted from the observed signals. Thus, for ARD under steady-state conditions, extremely high pumping rates are required on the collimator between the two slits separating the reaction chamber and the analyzer [83,157].

ARD work has frequently been performed with catalyzed reactions under non-steady-state conditions by means of modulated molecular beams (MMBs), TPD, TPR, or pressure jumps [17]. The signals from the products after AR procedures are so small that their detection sensitivities are frequently enhanced by modulation or transient techniques. For example, the supply of reactants is modulated to increase their detection sensitivity by using locking-amp techniques. The resultant reactant density on the surface will vary periodically. This may cause the reactant coverage to change throughout the conditions critical for chemical kinetics. In fact, no kinetic transition has ever been found in the CO oxidation by MMBs, although the kinetic transition itself is well reproduced in the steady-state CO oxidation on noble-metal surfaces [17,158]. The kinetic transition takes place at a definite CO/O_2 pressure ratio in a wide range of surface temperatures, and both the CO_2 desorption dynamics (spatial and velocity distributions) and its chemical kinetics (reaction orders and activation energy) behave differently below and above the transition point. The product desorption dynamics derived from MMBs will provide some ambiguities due to the reaction condition averaged over the scanned stages. Similar difficulties may occur when the modulation method is used for NO reduction by H_2 on Pd(110), Pd(211), or Rh(100). There is a critical kinetic transition where the N_2 emission channel switches sharply with increasing H_2 pressure (or surface temperature) from the decomposition of intermediate $N_2O(a) \rightarrow N_2(g)+O(a)$ to the associative process of nitrogen adatoms $2N(a) \rightarrow N_2(g)$ or to removal as ammonia [12,13,18]. In the former, the N_2 emission is off normal (two-directional), whereas in the latter, the product is desorbed along the surface normal or disappears. Without attention to these conditions, the modulation methods would provide desorption dynamics averaged over the above phenomena.

6. Inadequate Use of the Detailed Balance Principle

The DBP can be formulated as: ”at equilibrium, the rate of formation of a distinguishable macroscopic state and its reverse rate must be equal for a quantum

system governed by transitions of random phase" [159,160]. This is valid only at equilibrium because the principle comes from the second law of thermodynamics. For non-equilibrium, the DBP is applied for only quasi-equilibrium parts where the forward and reverse transition probabilities connecting two quantum states are equal. A similar principle, microscopic reversibility demands that if one reverses individual trajectories of elementary steps in space and time they must follow exactly the same trajectory. In other words, the same potential energy curve governs the interaction of a molecule-surface system regardless of whether the molecule is approaching the surface or leaving the surface [160]. These are all believed to be valid at equilibrium and we do not criticize this balancing. It should be noted that nobody obtains dynamic parameters controlling adsorption or desorption at equilibrium.

These principles have frequently been invoked in the field of desorption dynamics irrespectively of the above conditions; i.e., the DBP has often been invoked at far from equilibrium conditions. Especially, it has frequently been used in the desorption dynamics of hydrogen molecules on Cu surfaces, resulting in the unreasonable assumption of the desorption-angle independence of the internal energy of desorbing H_2 (or D_2) (without experimental confirmation) [20,21,27,28,30,79,161]; i.e., the use of this principle leads to the omission of the angle dependence of the EP into the rotational and translational modes in repulsive desorption because it partly replaces the parameters from non-AR desorption data with those derived from incident-angle-resolved adsorption data.

6. 1. Assumed Detailed Balance

It should be noted that the balance at equilibrium holds between the forward rate and the reverse one at each elementary step and not between their rate parameters (for example, the activation energies) for both directions. Similarly, the balance holds for the energy flows in both directions and not between parameters controlling the energy flows (for example, the energy partitioning). No proof has been found that justifies the use of adsorption parameters (such as the incident-angle dependence of an adsorption rate) instead of desorption parameters (such as the desorption-angle dependence of flux) of the reverse process [21,23]. Even if these replacements could be assumed, the current use of the DBP far from equilibrium is not justified because of the remarkable dependences of dynamic parameters on the desorption angle, surface structures, and amounts of surface species as explained below.

Actually, these adsorption (or desorption) parameters must be determined under conditions where adsorption is much faster than desorption (or vice versa). Generally, there are large differences in the experimental conditions between these two cases, for example, in the amount of surface species, the reaction (or surface) temperature, and the free energy decrement induced in each elementary process even when no surface structure changes. In the currently prevailing use of the DBP, these differences are neglected and the observed *adsorption (or desorption) parameters are assumed to be*

invariant even when the prevailing process shifts from adsorption to desorption or vice versa. Thus, use of the DBP for adsorption and its reverse desorption eventually leads to the supposition that dynamic parameters such as energy partitioning or distributions of product flux or energies (for the whole desorption as well as each component (if any)) remain invariant regardless of surface conditions.

This invariance is noticeably inconsistent with experimental facts. Some examples disputing this supposition are given below. In the literature, the spatial distribution of hyper-thermal products was first noticed to depend on the coverage of reactants (CO(a) + O(a)) with CO_2 desorption in CO oxidation on Pd(111), Pd(100), and Pd(110) [17,162]. The spatial distribution of desorbed CO_2 commonly becomes sharp, and its kinetic energy increases when the reactant coverage increases (Fig. 4). This is caused by compressed surface lattices of CO(a) and/or O(a) [17]. On Pt(111) and stepped Pt(332), two CO_2 desorption components (hyperthermal and thermal) differently contribute to the total product formation, depending on oxygen coverage and the surface temperature [163]. A remarkable example of the coverage dependence is found in the spatial distributions of product N_2 in the decomposition of $N_2O(a) \rightarrow N_2(g)+O(a)$ [18]. The distribution is sensitive to the $N_2O(a)$ coverage on Rh(100), Pd(110), Ir(110), and Rh(110). On Rh(100), the N_2 desorption is four-directional (off normal) with small N_2O coverage (Fig. 12) [16,146]. With increasing $N_2O(a)$ coverage, the N_2 desorption is accompanied by an additional component directed along the surface normal. This new component becomes major with high coverage. On Pd(110), Rh(110), and Ir(110), the two directional (off-normal) N_2 desorption is observed only at small $N_2O(a)$ coverage [18,145].

Second, Yamanaka's AR-IR emission analysis [8], reporting angle-dependent rotational energy, invalidates the above supposition. In fact, before his work [156], the internal energies of hyper-thermal products had been examined via REMPI-TOF, LIF, or IR emission in non-AR fashions [27-29,71,72,164,165]. The non-AR procedures neglect the desorption-angle dependences of both the internal and translational energies.

Third, in several desorption systems, remarkable anisotropy is found in the spatial distribution of desorbing products, for example, (i) $CO(a)+O(a) \rightarrow CO_2(g)$ on Pd(110)(1×1), (ii) $N_2O(a) \rightarrow N_2(g)+ O(a)$ on Pd(110)(1×1), Rh(110)(1×1), Rh(100)(1×1) and Ir(110)(1×1), and (iii) $2N(a) \rightarrow N_2(g)$ on Pd(110)(1×1) and Ir(110)(1×1) [14,17,18]. In these desorption systems, the symmetry of reaction sites or the orientation of intermediates is more or less memorized in the spatial distribution of desorbed products. Desorption dynamics must include some parameters that describe surface structures.

It is worthwhile to consider the reason it took such a long time (over half a century) to notice the inadequate use of the DBP in desorption dynamics. There seem to be two main reasons, i.e., (1) non-AR analysis of the rotational energy and (2) incomplete examinations of the DBP with the adsorption/desorption of H_2 (or D_2) on copper surfaces. The wrong presupposition has not been critically examined even after the population in each energy state of desorbed H_2 or D_2 has been analyzed by means of REMPI (in non-AR fashions). It is unfortunate that the applicability of the DBP was

examined only in H_2 (or D_2) adsorption/desorption on Cu(111) because this is not suitable as a proof system to examine desorption dynamics, as explained in Section 3-4.

Measuring the AR-TOF of desorbed species at each rotational state remains difficult experimentally speaking; therefore, there have been no simultaneous examinations of the rotational and translational energies versus the desorption angle. Instead, angle-independent rotational (or internal) energy has been tacitly assumed by using non-AR rotational energy distributions within the framework of the DBP. The desorption-angle dependence of the internal energy was first reported in 2008 by means of spectrum analysis of the IR emission from nascent CO_2 after AR procedures, but that work was still performed in a non-state-resolved way [8,156]. The confirmation of significant angle dependence of the rotational energy clearly shows inadequate use of the DBP but does not provide quantitative analysis of the desorption-angle dependence of the EP to rotational and translational modes. The desorption-angle dependence of the rotational energy would be more remarkable if the energy were analyzed in AR and state-selected ways.

The necessity of the concept of EP into the rotational and translational modes did not seem to be strong enough to perform new ARD experiments for the internal energy. Examination of the DBP had been limited to the adsorption/desorption of H_2 or D_2 on Cu(111) in which the translational energy exceptionally remains invariant with an increasing desorption angle. This might mislead to the angle-independent rotational energy without experiments. The translational energy seems invariant when the EP largely shifts to the translational mode. Indeed, it is unfortunate that the applicability of the DBP has not been examined with other desorption systems except for H_2/Cu, since EP into the rotational and translational modes is well known in gas-phase reaction dynamics [19].

6. 2. Confusion over the Detailed Balance Principle

Current use of the DBP originated from Willigen's model for the angular distribution of desorbing H_2 in the reverse process of activated (dissociative) adsorption [23]. There, the PES for dissociative adsorption of H_2 is assumed to have a barrier only along the surface normal (a flat barrier model). In this treatment, the internal energy modes of incident H_2 and desorbing H_2 are frozen, and only the normal velocity component of incident H_2 is assumed to be effective to surmount the activation energy barrier to dissociation. In the reverse process, the nascent H_2 jumps over this energy barrier to vacuum at the moment of association of H(a)+H(a). Here, it is assumed that the desorbing molecules hold the kinetic energy they had held before adsorption. In other words, desorbing species are only molecules with energy high enough to surmount the adsorption barrier. No other molecules with lower kinetic energy are involved.

Thus, the well-known Willigen's equation for angular distribution was derived by replacing *the desorption-angle* dependence of the flux of hyper-thermal product H_2 with *the incident-angle* dependence of the activated adsorption probability. This replacement

was essential in Willigen's report and remains in current use of the DBP even after the DBP has been extended to rotational and vibrational modes [20,28,79,161,166]. The extension was performed by replacing some dynamic parameters derived from AR-adsorption data with similar parameters obtained from non-AR desorption data (or vice versa) in the framework of the DBP [21]. The resultant model yields a high kinetic energy of the molecules emitted at large off-normal angles because the molecules at large *incident* angles must have a high kinetic energy to surmount the activation barrier because of the relatively small normal-velocity components. However, the observed translational energy of H_2 either decreases with the increasing desorption angle (on Ni(111)) or remains fairly invariant (on Cu(111) or Cu(100)) [25,27,28] (never increases!).

As described above, a similar decreasing kinetic energy is observed in the associative desorption of $CO(a)+O(a)\rightarrow CO_2(g)$ on Pt(111) [167] and Pd(110) [17] or $N(a)+N(a)\rightarrow N_2(g)$ on Pd(110) [18]. This remarkable inconsistency has apparently been dissolved by inserting *a width parameter* into the desorption parameters within the framework of the DBP [21,27,28,79,161]. The origin of the width parameter comes from the simulation of the dependence of the sticking probability on the internal and translational energies of incident H_2 as well as the incident angle. It apparently provides a distribution of the activation energy barrier height for H_2 adsorption in the dissociation probability curve versus the total energy of the incident molecules. However, its physical meaning remains unclear, since no explanations have been found for its use as one of the desorption parameters. Thus, the width parameter behaves as a buffer function, because the energy distribution of desorbed products is tacitly assumed to be independent of the desorption angle. Although such treatments with the DBP make explanations consistent, they also make the physics of the repulsive desorption ambiguous.

6. 3. Re-Examination of Hydrogen Desorption

In the past, the EP into the rotational and translational modes in repulsive desorption had a chance to be noticed, since the relation of the translational energy to the rotational energy was frequently discussed after non-AR-REMPI-TOF measurements of D_2 (or H_2) desorbing from Cu(111) [79,161]. The velocity of desorbing D_2 at each rotational (J) state and vibrational (v) state is widely distributed, and then the average translational energy is calculated. The results are partly reproduced from the data in Ref. 79, as plotted against the rotational energy at the ground vibrational (v=0) and first excited (v=1) states (the open symbols in Fig. 13). Similar results were reported for H_2 desorption on Cu(111) [161]. The data designated by the closed symbols have been reanalyzed 21 years after the former evaluations [166]. The new results were shifted upward by about 0.13 eV after the careful reanalysis of the raw data. It should be noted that, although the general feature remains invariant, there are large differences in the translational energy at small J values. In the former evaluations in 1993, the

translational energy first increased with increasing rotational energy below J=5 and then decreased above J=6. These dependences have long been explained within the framework of the DBP by using the dependence of *the dissociation probability of incident* D_2 on its rotational energy; i.e., the rotation below J=4 inhibits the dissociative adsorption by means of a steric hindrance, and the rotational energy above J=6 enhances the dissociation, reducing the translational energy necessary for dissociation [21,27,79]. These explanations have long been indispensable for maintaining the validity of the DBP. Here, the above *desorption phenomena are surprisingly explained by means of the concepts for adsorption.* Neither desorption nor energy partitioning in repulsion is involved. The steric (orientation) effect due to rotation is unlikely in repulsive desorption, although it is well-known as rainbow scattering in the adsorption direction [74-77]. The analysis revised in 2014 shows that the dependence below J=4 becomes unclear because of the scattered data.

On the other hand, with the EP model, the released energy in repulsive desorption is partitioned into different modes of desorbed species. At fixed vibrational states, the remaining energy is mostly partitioned into the rotational and translational modes, since the mass of D_2 is much smaller than that of metal atoms, suggesting more elastic repulsions. With this model, the sum of the translational and rotational energies should be nearly independent of the rotational state at a definite vibrational state. With increasing rotational energy, the translational energy is expected to linearly decrease with a slope of -1 (the blue line in Fig. 13). Actually, the averaged kinetic energy decreases with a slope of -0.4 for the ground vibrational state (v=0) above J=5 in both former and new analyses. The results are similar at the first excited vibrational state, yielding a slope of -0.4, except for J<5. The observed slopes are far from the expected value of -1.

This may be due to the translational energy averaged over the limited desorption angles (i.e., the acceptance angle of the used ion collector is limited to about ±20° [79]). In non-AR-REMPI-TOF, the translational energy is overestimated at higher rotational energies when the EP into the rotational and translational modes is operative, because the slower components with a definite rotational energy are more broadly distributed. The fraction of the slower components around the normal direction is decreased as compared with that at off-normal angles. The ion collector will receive the faster components more than those averaged over the whole angle. The resultant translational energy is overestimated more at higher rotational energies. Thus, the observed translational energy must decrease with increasing rotational energy more slowly than that with the expected slope in the EP model. The slope of the kinetic energy against the rotational energy must shift toward the expected value of -1 after AR-REMPI-TOF work. The kinetic energies at v=1 are generally smaller than those at v=0, indicating smaller repulsive forces, and the resultant EP will be different from that at v=0. In this case, coupling the rotation with the vibration will become more important than that at the ground state.

At small J values, the translational energy largely shifts from the EP model, since it should increase as the rotational energy decreases. The explanations of the translational energies at these small J values are troublesome in both the DBP and EP models. The

translational energy at small J values might be underestimated for two reasons: first, the energy is underestimated more at lower rotational energies by non-AR-REMPI-TOF, as explained above. Second, inadequate corrections may be due to the high background signals at small J values, especially below J =3. There are two peaks in a TOF spectrum at fixed J values. The fast component comes from desorbed D_2, and the slow one is due to the background gas at the same J value. These components partly overlap in TOF curves because the population at small J values in the ground vibrational state is relatively high in the background gas. In fact, there are some differences in the reported data from different laboratories [28,79,161,166].

In the case of D_2 or H_2 desorption on Cu(111) and Cu(110), the population at each rotational state decreases rapidly with increasing rotational energy [168]. This means that the released energy is highly transferred into the translational modes, yielding apparently angle-independent kinetic energy. The rotational energy, however, may increase at large off-normal angles even though the population is very small. This point should be quantitatively re-examined after AR internal energy measurements.

7. Summary

This review summarizes how angle-resolved desorption (ARD) has become surface-structure sensitive in the studies of NO and N_2O reduction. It also shows how inadequate use of the detailed balance principle (DBP) has prevented desorption dynamics from being sensitive to surface structures. The following points are emphasized.

1. The structure sensitivity of desorption dynamics is based on the anisotropic distributions of the energies and flux of hyper-thermal products.

2. Anisotropy is induced by either asymmetric structures around a desorption site or anisotropic energy partitioning (EP) in the repulsive desorption of hyper-thermal products into their translational and rotational modes. The extent of this EP is largely controlled by the orientation of a transition state against the surface plane.

3. Some results from ARD are inconsistent with current use of the DBP, in which the desorption-angle dependence of the internal energies is omitted. By this assumption, the usage of DBP makes the physical meaning of each desorption parameter related to surface structures ambiguous.

4. All of the energies of product molecules, as well as their flux, are examined as functions of desorption and azimuth angles in the next generation of ARD. For such analysis, new angle-resolved desorption measurements are proposed.

8. Acknowledgments

This work was partly supported by a 1996 Center of Excellence (COE) Special Equipment Program of the Ministry of Education, Sports, and Culture of Japan and by

Grant-in-Aid No. 21550004 for General Scientific Research from the Japan Society for the Promotion of Science (JSPS). A.K. acknowledges the financial support from the Slovenian Research Agency (Grant. No. P2-0393) and the JSPS for financing his research visits to Japan.

References

[1] P. Granger, V.I. Parvulescu, Catalytic NOx abatement systems for mobile sources: From three-way to lean burn after-treatment technologies, Chem. Rev. 111 (2011) 3155–3207.
[2] R. Zhang, N. Liu, Z. Lei, B. Chen, Selective transformation of various nitrogen-containing exhaust gases toward N_2 over zeolite catalysts, Chem. Rev. 116 (2016) 3658–3721.
[3] S. Roy, A. Baiker, NOx Storage−Reduction Catalysis: From Mechanism and Materials Properties to Storage−Reduction Performance, Chem. Rev. 109 (2009) 4054–4091.
[4] M. Haneda, I. Nakamura, T. Fujitani, H. Hamada, Catalytic active site for NO decomposition elucidated by surface science and real catalyst, Catal. Surv. Asia, 9 (2005) 207-215.
[5] V. I. Pârvulescu, P. Grange, B. Delmon, Catalytic removal of NO, Catal. Today, 46 (1998) 233-316.
[6] M. Balooch, R.E. Stickney, Angular distributions of H_2 desorbed from the (100), (110), and (111) faces of copper crystals, Surf. Sci. 44 (1974) 310-320.
[7] M. Balooch, M.J. Cardillo, D.R. Miller, R.E. Stickney, Molecular beam study of the apparent activation barrier associated with adsorption and desorption of hydrogen on copper, Surf. Sci. 46 (1974) 358-392.
[8] T. Yamanaka, T. Matsushima, Polar- and azimuth-angle-dependent rotational and vibrational excitation of desorbing product CO_2 in CO oxidation on palladium surfaces, Phys. Rev. Lett. 100 (2008) 026104(1-4).
[9] T. Matsushima, H. Orita, A. Kokalj, An experimental approach to transition states of surface reactions; energy partitioning in repulsive desorption, e-J. Surf. Sci. Nanotech. 11 (2013) 65-71.
[10] T. Matsushima, A. Kokalj, Angular distributions of desorbing N_2 in thermal N_2O decomposition on Rh(100), Surf. Sci. 601 (2007) 3996-4000.
[11] H. Orita, T. Kubo, T. Matsushima, A. Kokalj, DFT calculations of adsorption and decomposition of N_2O on Rh(100), |J. Phys. Chem. C, 114 (2010) 21444–21449.
[12]. T. Matsushima, A. Kokalj, N_2 emission via intermediate N_2O in a steady-state NO+CO+D_2 reaction on stepped Pd(211) by angle-resolved desorption, J. Phys. Chem. C, 119 (2015) 11699-11713.
[13] T. Matsushima, A. Kokalj, H. Orita, T. Kubo, M. Sakurai, T. Kondo, J. Nakamura, N_2 Emission-channel change in NO reduction over stepped Pd(211) by angle-resolved desorption. Surf. Sci. 606 (2012) 1029–1036.
[14] T. Matsushima, K. Shobatake, Surface reaction dynamics and energy partitioning, J. Mol. Catal. A, Chemical. 315 (2010) 135–147.
[15] T. Matsushima, A. Kokalj, N_2 emission in steady-state N_2O+CO and NO+CO reactions on Ir(110) by means of angle-resolved desorption, Appl. Surf. Sci. 414 (2017) 153-162.
[16] T. Kondo, M. Sakurai, T. Matsushima, J. Nakamura, Angle resolved intensity and

velocity distributions of N_2 desorbed by N_2O decomposition on Rh(110), J. Chem. Phys. 132 (2010) 134704(1-9).
[17] T. Matsushima, Angle-resolved measurements of product desorption and reaction dynamics on individual sites, Surf. Sci. Rep. 52 (2003) 1-62.
[18] T. Matsushima, Surface structural information carried by desorbing reaction products. Prog. Surf. Sci. 82 (2007) 435-477.
[19] J.C. Polanyi, Concepts in reaction dynamics, Acc. Chem. Res. 5 (1972) 161-168.
[20] C.T. Rettner, D.J. Auerbach, J.C. Tully, A.W. Kleyn, Chemical dynamics at the gas−surface interface, J. Phys. Chem. 100 (1996)13021-13033.
[21] H.A. Michelsen, D.J. Auerbach, A critical examination of data on the dissociative adsorption and associative desorption of hydrogen at copper surfaces, J. Chem. Phys. 94 (1991) 7502-7520.
[22] D.-J. Liu, J.W. Evans, Realistic multisite lattice-gas modeling and KMC simulation of catalytic surface reactions: Kinetics and multiscale spatial behavior for CO-oxidation on metal (100) surfaces, Prog. Surf. Sci. 88 (2013) 393-521.
[23] W. van Willigen, Angular distribution of hydrogen molecules desorbed from metal surfaces, Phys. Lett. 28A (1968) 80–81.
[24] H. Ueba, Vibrational lineshapes of adsorbates on solid surfaces, Prog. Surf. Sci. 22 (1986) 181-321.
[25] G. Comsa, R. David, Dynamical parameters of desorbing molecules, Surf. Sci. Rep. 5 (1985) 145–198.
[26] R.R. Cavanagh, E.J. Heilweil, J.C. Stephenson, Time-resolved probes of surface dynamics, Surf. Sci. 283 (1993) 226-232.
[27] H.A. Michelsen, C.T. Rettner, D.J. Auerbach, The adsorption of hydrogen at copper surfaces: a model system for the study of activated adsorption, in Springer Series in Surface Sciences, Surface Reactions, Ed. R.J. Madix, Vol. 34 (Springer-Verlag, Berlin, 1994) p. 185-237.
[28] A. Hodgson, State resolved desorption measurements as a probe of surface reactions, Prog. Surf. Sci. 63 (2000) 1-61.
[29] D. Wetzig, R. Dopheide, M. Rutkowski, R. David, H. Zacharias, Rotational alignment in associative desorption of D_2(v= 0 and 1) from Pd(100), Phys. Rev. Lett. 76 (1996) 463-466.
[30] A.M. Wodtke, Electronically non-adiabatic influences in surface chemistry and dynamics, Chem. Soc. Rev. 45 (2016) 3641-3157.
[31] P. Casavecchia, Chemical reaction dynamics with molecular beams. Rep. Prog. Phys. 63 (2000) 355-414.
[32] T. Matsushima, Anisotropic angular distribution of desorption of CO_2 produced on Pd(110) surfaces, Chem. Phys. Lett. 155 (1989) 313-316.
[33] Y. Ma, T. Matsushima, K. Shobatake, A. Kokalj, Spatial distributions of desorbing products in steady-state NO and N_2O reductions on Pd(110), J. Chem. Phys. 124 (2006) 144711(1-11).

[34] A. Groβ, Reactions at surfaces studied by ab initio dynamics, Surf. Sci. Rep. 32 (1998) 291-340.
[35] R.A. van Santen, M. Neurock, S.G. Shetty, Reactivity theory of transition-metal surfaces: a Brønsted-Evans-Polanyi linear activation energy-free-energy analysis, Chem. Rev. 110 (2010) 2005–2048.
[36] H.S.Taylor, A theory of the catalytic surface, Proc. Roy. Soc. A 108 (1925) 105-111.
[37] C.S. Tian, Y.R. Shen, Recent progress on sum-frequency spectroscopy, Surf. Sci. Rep. 69 (2014) 105-131.
[38] A. Savara, E. Weitz, Elucidation of intermediates and mechanisms in heterogeneous catalysis using infrared spectroscopy, Annu. Rev. Phys. Chem. 65 (2014) 249-273.
[39] A. Baraldi, G. Comelli, S. Lizzit, M. Kiskinova, G. Paolucci, Real-time X-ray photoelectron spectroscopy of surface reactions, Surf. Sci. Rep. 49 (2003) 169-224.
[40] C. Westphal, The study of the local atomic structure by means of X-ray photoelectron diffraction, Surf. Sci. Rep. 50 (2003) 1-106.
[41] D.P. Woodruf, Adsorbate structure determination using photoelectron diffraction: Methods and applications, Surf. Sci. Rep. 62 (2007) 1-38.
[42] F. Besenbacher, J.K. Nørskov, Oxygen chemisorption on metal surfaces: General trends for Cu, Ni and Ag, Prog. Surf. Sci. 44 (1993) 5-66.
[43] F. Rosei, M. Schunack, Y. Naitoh, P. Jiang, A. Gourdon, E. Laegsgaard, I. Stensgaard, C. Joachim, F. Besenbacher, Properties of large organic molecules on metal surfaces, Prog. Surf. Sci. 71 (2003) 95-146.
[44] B.R. Cuenya, F. Behafarid; Nanocatalysis: size- and shape-dependent chemisorption and catalytic reactivity, Surf. Sci. Rep. 70(2015) 135-187.
[45] R.D. Levine, R.B. Bernstein, Molecular reaction dynamics, (Oxford University Press, Oxford, 1974).
[46] J.C. Polanyi, A.H. Zewail, Direct observation of the transition state, Acc. Chem. Res. 28 (1995) 119–132.
[47] H. Ulbricht, R. Zacharia, N. Cindir, T. Hertel, Thermal desorption of gases and solvents from graphite and carbon nanotube surfaces, Carbon, 44 (2006) 2931–2942.
[48] H. Ueba, Vibrational relaxation and pump-probe spectroscopies of adsorbates on solid surfaces. Prog. Surf. Sci. 55 (1997) 115-179.
[49] H. Arnolds, M. Bonn, Ultrafast Surface Vibrational Dynamics, Surf. Sci. Rep. 65 (2010) 45-66.
[50] K. Watanabe, A. Kokalj, Y. Inokuchi, I.I. Rzeznicka, K. Ohshimo, N. Nishi, T. Matsushima, Orientation of nitrous oxide on palladium(110) by STM, Chem. Phys. Lett. 406 (2005) 474–478.
[51] K. Watanabe, A. Kokalj, H. Horino, I.I. Rzeznicka, K. Takahashi, N. Nishi, T. Matsushima, Scanning-tunneling microscopy, near-edge X-ray-absorption fine structure, and density-functional theory studies of N_2O orientation on Pd(110), Jpn. J. Appl. Phys. 45(3B) (2006) 2290–2294.

[52] W.A. Brown, P. Gardner, D.A. King, Very low temperature surface reaction: N_2O formation from NO dimers at 70 to 90 K on Ag{ 111}, J. Phys. Chem. 99 (1995) 7065-7074.
[53] W.A. Brown, R.K. Sharma, D.A. King, S. Haq, Adsorption and reactivity of NO and N_2O on Cu{110}: Combined RAIRS and molecular beam studies, J. Phys. Chem. 100 (1996) 12559-12568.
[54] E. Ozensoy, C. Hess, D.W. Goodman, Isocyanate formation in the catalytic reaction of CO +NO on Pd(111): An in situ infrared spectroscopic study at elevated pressures, J. Am. Chem. Soc. 124 (2002) 8524-8525.
[55] E. Ozensoy, D.W. Goodman, Vibrational spectroscopic studies on CO adsorption, NO adsorption, CO+NO reaction on Pd model catalysts, Phys. Chem. Chem. Phys. 6 (2004) 3765-3778.
[56] W.A. Brown, P. Gardner, M. Perez Jigato, D. A. King, Characterization and orientation of adsorbed NO dimers on Ag{111} at low temperatures, J. Chem. Phys. 102 (18), (1995) 7277-7280.
[57] Z.-P. Liu, S.J. Jenkins, D.A. King, Why is silver catalytically active for NO reduction? A unique pathway via an inverted $(NO)_2$ dimer, J. Am. Chem. Soc. 126 (2004) 7336-7340.
[58] C.I. Carlisle, D.A. King, Direct molecular imaging of NO monomers and dimers and a surface reaction on Ag{111}. J. Phys. Chem. B, 105 (2001) 3886-3893.
[59] C. Hess, E. Ozensoy, C.-W. Yi, D. W. Goodman, NO Dimer and Dinitrosyl Formation on Pd(111): From Ultra-High-Vacuum to Elevated Pressure Conditions, J. Am. Chem. Soc. 128, (2006) 2988-2994.
[60] H. Wang, R.G. Tobin, C.L. DiMaggio, G.B. Fisher, D.K. Lambert, Reactions of N and NO on Pt(335), J. Chem. Phys. 107 (1997) 9569-9576.
[61] D.N. Belton, C.L. DiMaggio, S.J. Schmieg, K.Y. Simon Ng, Reaction of Coadsorbed Nitric Oxide and Nitrogen Atoms on Rh(111), J. Catal. 157 (1995) 559-568.
[62] M. Ikai, K.-I. Tanaka, Mechanism for the off-normal emission of N_2 in the desorption-mediated reaction of NO on a Pd(110) surface, J. Phys. Chem. B, 103 (1999) 8277−8282.
[63] M. Ikai, K.-I. Tanaka, Spatial distribution of N_2, N_2O, and NO desorbing from a Pd(211) surface, J. Chem. Phys. 110 (1999) 7032-7036.
[64] V.P. Zhdanov, B. Kasemo, Mechanism and kinetics of the NO+CO reaction on Rh, Surf. Sci. Rep. 29 (1997) 31-90.
[65] S. Carré, C. Dujardin, P. Granger, Operando infrared spectroscopy of the reduction of NO by H_2 over rhodium based catalysts, Catal. Today, 191 (2012) 59-64.
[66] G. Centi, G.E. Arena, S. Perathoner, Nanostructured catalysts for NOx storage–reduction and N_2O decomposition, J. Catal. 216 (2003) 443-454.
[67] C.T. Campbell, J.M. White, Chemisorption and reactions of nitric oxide on rhodium, Appl. Surf Sci. 1 (1978) 347-359.
[68] T.W. Root, L.D. Schmidt, G.B. Fisher, Adsorption and reaction of nitric oxide and

oxygen on Rh(111), Surf. Sci. 134 (1983) 30–45.
[69] B.K. Cho, Mechanistic importance of intermediate N_2O + CO reaction in overall NO + CO reaction system: I. Kinetic analysis, J. Catal. 138 (1992) 255-266.
[70] H. Permana, K.Y. Simon Ng, C.H.F. Peden, S.J. Schmieg, D.K. Lambert, D.N. Belton, Adsorbed species and reaction rates for NO–CO over Rh(111), J. Catal. 164 (1996) 194-206.
[71] L. Schröter, Chr.Trame, R. David, H. Zacharias, State specific velocity distribution of hydrogen isotopes desorbing from Pd(100), Surf. Sci. 272 (1992) 229-234.
[72] K. Nakao, O. Watanabe, T. Sasaki, S. Ito, K. Kunimori, CO oxidation on Pd(111), Pt(111), and Rh(111) surfaces studied by infrared chemiluminescence spectroscopy, Surf. Sci. 601 (2007) 3796-3800.
[73] A. Hodgson, State-resolved measurements of surface reaction dynamics. in Surface Dynamics, Ed. D.P. Woodruff (Elsevier, 2003), Chapter 6. p143-175.
[74] G.O. Sitz, A.C. Kummel, R.N. Zare, J.C. Tully, Direct inelastic scattering of N_2 from Ag(111). II. Orientation, J. Chem. Phys. 89 (1988) 2572-2582;
[75] J.L.W. Siders, G.O. Sitz, Observation and characterization of direct inelastic and trapping-desorption channels in the scattering of N_2 from Cu(110), J. Chem. Phys. 101 (1994) 6264-6270.
[76] C.M. Matthews, F. Balzer, A.J. Hallock, M.D. Ellison, R.N. Zare, Scattering of N_2 from Ni(111), Surf. Sci. 460 (2000) 12–20.
[77] G.O. Sitz, Inelastic scattering of heavy molecules from surfaces, Handbook of surface science, volume 3, (edited by E. Hasselbrink and B.I. Lundqvist, Elsevier 2008) chapter 6, page 197-229.
[78] M.P. Jigato, WK. Walter, D.A. King, The temperature dependent effect of adsorbate hindered vibrations on NEXAFS analyses: NO on Pd{110}, Surf. Sci. 301 (1994) 273-284.
[79] H.A. Michelsen, C.T. Rettner, D.J. Auerbach, R.N. Zare, Effect of rotation on the translational and vibrational energy dependence of the dissociative adsorption of D_2 on Cu(111). J. Chem. Phys. 98 (1993) 8294-8307;
[80] T. Matsushima, K. Shobatake, Y. Ohno, K. Tabayashi. Anisotropic velocity distribution of desorbing product in carbon monoxide oxidation on palladium(110), J. Chem. Phys. 97 (1992) 2783-2789.
[81] T. Matsushima, The crystal azimuth dependence of the angular distribution of the desorption flux of carbon dioxide produced on palladium(110) surfaces, J. Chem. Phys. 91 (1989) 5722-5730.
[82] A. Alavi, P. Hu, T, Deutsch, P.L. Silvestrelli, J. Hutter, CO Oxidation on Pt(111): An ab initio density functional theory study, Phys. Rev. Lett. 80 (1998) 3650-3653.
[83] M. Kobayashi, Y. Tuzi, Performance of a directional detector of molecular density, J. Vac. Sci. Technol. 16 (1979) 685–688.
[84] T. Matsushima, Crystal azimuth dependence of the desorption flux of carbon dioxide produced on palladium (110) and (111) surfaces, Vacuum, 41 (1990) 275-277.

[85] Y. Ohno, T. Matsushima, Spatial distribution of reactive carbon dioxide desorption on palladium(100) surfaces, Surf. Sci. 239 (1990) L521-L525.
[86] M. Wu, P.M. Johnson, A study of some Rydberg states of CO_2 by (3+1) multiphoton ionization spectroscopy, J. Chem. Phys. 91 (1989) 7399-7407.
[87] I.I. Rzez´nicka, Y.-S. Ma, G.-G. Cao, T. Matsushima, Removal pathways of surface nitrogen in a steady-state NO + CO reaction on Pd(110) and Rh(110): angular and velocity distribution studies, J. Phys. Chem. B 2004, 108 (2004) 14232-14243.
[88] O. Hinrichsen, F. Rosowski, A. Hornung, M. Muhler, G. Ertl, The kinetics of ammonia synthesis over Ru-Based catalysts: 1. The dissociative chemisorption and associative desorption of N_2, J. Catal. 165 (1997) 33-44.
[89] A. Nielsen, Latest developments in ammonia synthesis, Adv. Catal. 5 (1953) 1-37.
[90] B.K. Cho, B.H. Shanks, J.E. Bailey, Kinetics of NO reduction by CO over supported rhodium catalysts: Isotopic cycling experiments, J. Catal. 115 (1989) 486−499.
[91] K.I. Tanaka, Spatial distribution of molecules desorbing with surface reaction, in *Dynamic chemical processes on solid surfaces ; Chemical reactions and catalysis*" Springer Singapore (2017) page 85-95.
[92] Y. Ohno, K. Kimura, M. Bi, T. Matsushima, The translational energy of desorbing products in NO and N_2O decomposition on Pd (110), J. Chem. Phys. 110 (1999) 8221-8224.
[93] F. Zaera, C.S. Gopinath, Evidence for an N_2O intermediate in the catalytic reduction of NO to N_2 on rhodium surfaces, Chem. Phys. Lett. 332 (2000) 209-214.
[94] V. Bustos, C. S. Gopinath, R. Uñac, F. Zaera, G. Zgrablich, Lattice-gas study of the kinetics of catalytic conversion of NO–CO mixtures on rhodium surfaces, J. Chem. Phys. 114 (2001) 10927-10931.
[95] V. Bustos, R. Uñac, F. Zaera, Lattice-gas study of the kinetics of the catalytic NO–CO reaction on rhodium surfaces. II. The effect of nitrogen surface islands, J. Chem. Phys. 118 (2003) 9372- 9379
[96] D.N. Belton, C.L. Dimaggio, K.Y.S. Ng, N + N → N_2 Reaction Rates on Rh(111), J. Catal. 144 (1993) 273-284.
[97] I. Nakai, H. Kondoh, T. Shimada, M. Nagasaka, R. Yokota, T. Katayama, K. Amemiya, H. Orita, T. Ohta, Mechanism of N + NO reaction on Rh(111) surfaces: A precursor-mediated reaction, J. Phys. Chem. C, 113 (2009) 13257–13265.
[98] I. Nakai, H. Kondoh, T. Shimada, M. Nagasaka, R. Yokota, K. Amemiya, H. Orita, T. Ohta, N+NO reaction on Rh(111) surfaces studied with fast near-edge X-ray absorption fine structure spectroscopy: Role of NO dimer as an extrinsic precursor. J. Phys. Chem. B Lett. 110 (2006) 25578-25581.
[99] Y. Li, M. Bowker, The adsorption and decomposition of nitrous oxide on Rh(110) and Rh(111), Surf. Sci. 348 (1996) 67−76.

[100] M. L. Unland, Isocyanate intermediates in the reaction nitrogen monoxide + carbon monoxide over a platinum/aluminum oxide catalyst, J. Phys. Chem. 77 (1973) 1952-1956.
[101] H. Arai, H. Tominaga, An infrared study of nitric oxide adsorbed on rhodium-alumina catalyst, J. Catal. 43 (1976) 131-142.
[102] C. Hess, E. Ozensoy, D. W. Goodman, Combined in Situ Infrared and Kinetic Study of the Catalytic CO + NO Reaction on Pd(111) at Pressures up to 240 mbar, J. Phys. Chem. B, 107 (2003) 2759–2764.
[103] C. Hess, E. Ozensoy, C.-W. Yi, D. W. Goodman, NO Dimer and Dinitrosyl Formation on Pd(111): From Ultra-High-Vacuum to Elevated Pressure Conditions, J. Am. Chem. Soc. 128 (2006) 2988-2994.
[104] M. Ikai, H. He, C.E. Borroni-Bird, H. Hirano, K.I. Tanaka, Off-normal emission of N_2 produced by desorption mediated reaction of NO on Pd(110) surface, Surf. Sci. 315 (1994) L973-L976.
[105] M. Ikai, K.I. Tanaka, Off-normal emission of N_2 and normal emission of N_2O produced by the desorption mediated reaction of NO on Pd(110), Surf. Sci. 357/358 (1996) 781–785.
[106] K.I.Tanaka, M. Ikai, Adsorbed atoms and molecules destined for a reaction, Top. Catal. 20 (2002) 25−33.
[107] S. Haq, A. Hodgson, N_2O adsorption and reaction at Pd(110). Surf. Sci. 463 (2000) 1−10.
[108] P. Granger, C. Dujardin, J.F. Paul, G. Leclercq, An overview of kinetic and spectroscopic investigations on three-way catalysts: Mechanistic aspects of the CO+NO and CO+N_2O reactions, J. Mol. Catal. A, Chem. 228 (2005) 241–253.
[109] B.K. Cho, Mechanistic importance of intermediate N_2O + CO reaction in overall NO + CO reaction system: II. Further analysis and experimental observations, J. Catal. 148 (1994) 697−708.
[110] A.V. Zeigarnik, Adsorption and reactions of N_2O on transition metal surfaces. Kinet. Catal. 44 (2003) 233−246.
[111] Y. Ohno, I. Kobal, H. Horino, I.I. Rzeznicka, T. Matsushima, Desorption dynamics in N_2O decomposition on Pd(110), Appl. Surf. Sci. 169/170 (2001) 273-276.
[112] Kobal, I.; Kokalj, A.; Horino, H.; Ohno, Y.; Matsushima, T.; Surface-nitrogen removal studied from desorption dynamics. Trends Chem. Phys. 10 (2002) 139−178.
[113] T. Matsushima, N_2 emission in NO and N_2O reduction on Rh(100) and Rh(110), Phys. Chem. Chem. Phys. 9 (2007) 3031–3042.
[114] Y. Ma, T. Matsushima, Surface-nitrogen removal in a steady-state NO + H_2 reaction on Pd(110). J. Phys. Chem. B, 109 (2005) 1256-1261.
[115] A. Kokalj, I. Kobal, H. Horino, Y. Ohno, T. Matsushima, Orientation of N_2O molecule on Pd(110) surface, Surf. Sci. 506 (2002) 196−202.
[116] J.A. Herron, S. Tonelli, M. Mavrikakis, Atomic and molecular adsorption on Pd(111), Surf. Sci. 606 (2012) 1670-1679.

[117] A. Kokalj, I. Kobal, T. Matsushima, A DFT study of the structures of N_2O Adsorbed on the Pd(110) surface, J. Phys. Chem. B, 107 (2003) 2741−2747. (46)
[118] K. Watanabe, A. Kokalj, Y. Inokuchi, I.I. Rzeznicka, K. Ohshimo, N. Nishi, T. Matsushima, Orientation of nitrous oxide on palladium(110) by STM, Chem. Phys. Lett 406 (2005) 474-478.
[119] K. Watanabe, A. Kokalj, H. Horino, I. Rzeznicka, K. Takahashi, N. Nishi, T. Matsushima, Scanning-tunneling microscopy, near-edge X-ray-absorption fine structure, and density-functional theory studies of N_2O orientation on Pd(110), Jpn. J. Appl. Phys. 45 (2006) 2290-2294.
[120] H. Kawano, Effective work functions for ionic and electronic emissions from mono- and polycrystalline surfaces, Prog. Surf. Sci. 83, 1 (2008) 1-165.
[121] M. Sakurai, T. Matsushima, T. Kondo, J. Nakamura, Spatial distribution of desorbing N_2 in thermal decomposition of N_2O on stepped Pd(112), Proc. of 106-th Catal. Soc. Jpn. Meeting A, 2010, p. 4H14, (in Japanese).
[122] D.C. McCalman, K.H. Kelley, C.J. Werth, J.R. Shapley, W.F. Schneider, Aqueous N_2O reduction with H_2 over Pd-based catalyst: Mechanistic insights from experiment and simulation, Top. Catal. 55 (2012) 300−312.
[123] R. Burch, S.T. Daniells, J. P. Breen, P. Hu, A combined transient and computational study of the dissociation of N_2O on platinum catalysts, J. Catal. 252 (2004)252-260.
[124] H. Orita, N. Itoh, Adsorption of N_2 and N_2O on Ni(755) surface: ab initio periodic density functional study, Surf. Sci. 550 (2004) 166-176.
[125] J.M. Ricart, F. Ample, A. Clotet, D. Curulla, J.W. (Hans) Niemantsverdriet, J.F. Paul, J. Pérez-Ramírez, Structure and catalytic processes of N-containing species on Rh(111) from First Principles, J. Catal. 232 (2005)179–185.
[126] A. Kokalj, T. Matsushima, A density-functional theory study of the interaction of N_2O with Rh(110), J. Chem. Phys. 122 (2005) 034708(1-11).
[127] C.-Z. He, H. Wang, P. Zhu, J.-Y. Liu, Adsorption and dissociation of NO on Ir(100): a First-Principles study, J. Chem. Phys. 135 (2011) 204707 (1–7).
[128] W.B. Tolman, Binding and activation of N_2O at transition-metal centers: Recent mechanistic insights, Angew. Chem. Int. Ed. 49 (2010) 1018–1024.
[129] K. Imamura; T. Matsushima, N_2 desorption in the isothermal decomposition of N_2O on Rh(110) at low temperatures, Catal. Lett. 97 (2004) 197-202.
[130] S. Carré, C. Dujardin, P. Granger, Operando infrared spectroscopy of the reduction of NO by H_2 over rhodium based catalysts, Catal. Today, 191 (2012) 59-64.
[131] N.W. Cant, D.E. Angove, D.C. Chambers, Nitrous oxide formation during the reaction of simulated exhaust streams over rhodium, platinum and palladium catalysts, Appl. Catal. B: Environ. 17 (1998) 63-73.
[132] G. Centi, G.E. Arena, S. Perathoner, Nanostructured catalysts for NOx storage–reduction and N_2O decomposition, J. Catal. 216 (2003) 443-454.
[133] S.M. Vesecky, P.J. Chen, X.P. Xu, D.W. Goodman, Evidence for structure

sensitivity in the high pressure CO+NO reaction over Pd(111) and Pd(100), J. Vac. Sci. Technol. A 13 (1995) 1539−1543.
[134] S.M. Vesecky, D.R. Rainer, D.W. Goodman, Basis for the structure sensitivity of the CO+NO reaction on palladium, J. Vac. Sci. Technol. A 14 (1996) 1457−1463.
[135] D.R. Rainer, M. Koranne, S.M. Vesecky, D.W. Goodman, $CO+O_2$ and CO+NO reactions over Pd/Al_2O_3 catalysts, J. Phys. Chem. B, 101 (1997) 10769−10774.
[136] G.S. Herman, C.H.F. Peden, S.J. Schmieg, D.N. Belton, A comparison of the NO−CO reaction over Rh(100), Rh(110) and Rh(111), Catal. Lett. 62 (1999) 131−138.
[137] F. Gao, Y. Wang, D.W. Goodman, CO/NO and $CO/NO/O_2$ reactions over a Au−Pd single crystal catalyst, J. Catal. 268 (2009) 115−121.
[138] M.V. Castegnaro, A.S. Kilian, I.M. Baibich, M.C.M. Alves, J. Morais, On the reactivity of carbon supported Pd nanoparticles during NO reduction: Unraveling a metal−support redox interaction, Langmuir, 29 (2013) 7125−7133.
[139] J.R. Renzas, W. Huang, Y. Zhang, M.E. Grass, G.A. Somorjai, $Rh_{1-2x}Pd_x$ nanoparticle composition dependence in CO oxidation by NO, Catal. Lett. 141 (2011) 235−241.
[140] D.R. Rainer, S.M. Vesecky, M. Koranne, W.S. Oh, D.W. Goodman, The CO+NO reaction over Pd: A combined study using single-crystal, planar-model-supported, and high-surface-area Pd/Al_2O_3 catalysts, J. Catal. 167 (1997) 234−241.
[141] N.R. Avery, An EELS study of N_2O adsorption on Pt(111), Surf. Sci. 131 (1983) 501-510.
[142] J.C.L. Cornish, N.R. Avery, Adsorption of N_2, O_2, N_2O and NO on Ir(111) by EELS and TPD, Surf. Sci. 235 (1990) 209-216.
[143] P. Väterlein, T. Krause, M. Bäßler, R. Fink, E. Umbach, J. Taborski, V. Wüstenhagen, W. Wurth, Adsorption-induced bending of a triatomic molecule: Near-edge X-ray absorption fine-structure spectroscopy investiation of N_2O adsorbed on different Ni(111) surfaces. Phys. Rev. Lett. 76 (1996) 4749−4752.
[144] D.E. Beck, J.M. Heitzinger, A. Avoyan, B.E. Koel, Tuning the chemistry of metal surfaces: I. adsorption and reaction of NO and N_2O on ultrathin Pd films on Ta(110), Surf. Sci. 491 (2001) 48−62.
[145] H. Horino, I.I. Rzeznicka, A. Kokalj, I. Kobal, Y. Ohno, A. Hiratsuka, T. Matsushima, Two-directional N_2 desorption in thermal dissociation of N_2O on Rh(110), Ir(110), and Pd(110) at low temperatures, J. Vac. Sci. Technol. A, 20 (2002) 1592-1596.
[146] T. Matsushima, N_2 desorption in thermal N_2O decomposition on Rh(100), J. Phys. Chem. C, 111 (2007) 6422-6427.
[147] H.H. Huang, C.S. Seet, Z. Zou, G.Q. Xu, The adsorption of N_2O on clean and chemically modified Ru(001) surfaces, Surf. Sci. 356 (1996) 181-188.
[148] K. Imamura, H. Horino, I.I. Rzeźnicka, I. Kobal, A. Kokalj, Y. Ohno, B.E. Nieuwenhuys, A. Hiratsuka, T. Matsushima, Multi-directional N_2 desorption in N_2O decomposition on Rh(110), Surf. Sci. 566/568 (2004) 1076–1081.
[149] V.P. Zhdanov, T. Matsushima, Simulation of thermal desorption spectra of N_2

observed during N_2O decomposition on Rh(110), Surf. Sci. 583 (2005) 253–264.
[150] V.P. Zhdanov, T. Matsushima, Simulation of thermal desorption spectra of N_2 observed during N_2O decomposition on Rh(100), Surf. Sci. 601 (2007) 2373–2377.
[151] R. Schwarzwald. A. Mödi, T.J. Chuang, Two dimensional imaging of photodesorbed species from surfaces and the desorption dynamics, Surf. Sci. 242 (1991) 437-443.
[152] A.R. Burns, Quantum-resolved angular distributions of neutral products in electron-stimulated processes: Desorption of CO* from Pt(111), Surf. Sci. 280 (1995) 349–358.
[153] Q. Ran, D. Matsiev, A.M. Wodtke, D.J. Auerbach, An advanced molecule-surface scattering instrument for study of vibrational energy transfer in gas-solid collisions, Rev. Sci. Instrum. 78 (2007) 104104 (1-8).
[154] T. Engel, G. Ertl, Elementary steps in the catalytic oxidation of carbon monoxide on platinum metals, Adv. Catal. 28 (1979) 1-78.
[155] D.J. Harding, J. Neugebohren, H. Hahn, D.J. Auerbach, T.N. Kitsopoulos, A.M. Wodtke, Ion and velocity map imaging for surface dynamics and kinetics, J. Chem. Phys. 147 (2017) 013939 (1-7).
[156] T. Yamanaka, T. Matsushima, Internal-energy measurements of angle-resolved product CO_2 in catalytic CO oxidation by means of infrared chemiluminescence, Rev. Sci. Instrum. 78 (2007) 034105(1-6).
[157] T. Matsushima, K. Shobatake, Catalytic reactions studied by angle-resolved product desorption. *Catalysis* (published by the royal society of chemistry) 23 (2010) 139–178.
[158] Md. G. Moula, S. Wako, G. Cao, K. Kimura, Y. Ohno, I. Kobal, T. Matsushima, Two desorption components of product CO_2 in steady-state CO oxidation on Pd(110), Phys. Chem. Chem. Phys. 1 (1999) 3677-3683.
[159] A.N. Gorban, Detailed balance in micro- and macrokinetics and micro-distinguishability of macro-processes, Results in Physics, 4 (2014) 142–147.
[160] K. W. Kolasinski, Micrscopic reversibility in ad/desorption phenomena, in *Surface Science* (John-Wiley & Sons, Ltd. Baffins Lane, 2002) page 120-125.
[161] C.T. Rettner, H.A. Michelsen, D.J. Auerbach, Quantum state specific dynamics of the dissociative adsorption and associative desorption of H_2 at a Cu(111) surface, J. Chem. Phys. 102 (1995) 4625-4641.
[162] T. Matsushima, Angular resolved desorption, Hetero. Chem. Rev. 2 (1995) 51-68.
[163] J. Neugebohren, D. Borodin, H.W. Hahn, J. Altschäffel, A. Kandratsenka, D.J. Auerbach, C.T. Campbell, D. Schwarzer, D.J. Harding, A.M. Wodtke, T.N. Kitsopoulos, Velocity-resolved kinetics of site-specific carbon monoxide oxidation on platinum surfaces, Nature 558 (2018) 280-283, and its supplement.
[164] H. Uetsuka, K. Watanabe, H. Ohnuma, K. Kunimori, Infrared chemiluminescence study of the dynamics of steady-state CO oxidation on single-crystal Pd surfaces: effect of oxygen pretreatment, Surf. Sci. 377–379 (1997) 765-769.

[165] D.A. Mantell, S.B. Ryali, B.L. Halpern, G.L. Haller, J.B. Fenn, The exciting oxidation of CO on Pt, Chem. Phys. Lett. 81(1981) 185-187.
[166] F. Nattino, A. Genova, M. Guijt, A.S. Muzas, C. Díaz, D.J. Auerbach, G.-J. Kroes, Dissociation and recombination of D_2 on Cu(111): Ab initio molecular dynamics calculations and improved analysis of desorption experiments, J. Chem. Phys. 141 (2014) 124705 (1-14).
[167] J.A. Barker, D.J. Auerbach, Gas-surface interactions and dynamics; Thermal energy atomic and molecular beam studies, Surf. Sci. Rep. 4 (1984) 1-99.
[168] G.D. Kubiak, G.O. Sitz, R.N. Zare, Recombinative desorption of H_2 and D_2 from Cu(110) and Cu(111): Determination of nonequilibrium rovibrational distributions. J. Chem. Phys. 81 (1984) 6397-6398.

Figure Captions

Fig. 1. Three-dimensional spatial distribution (on polar coordinates) of desorbing product N_2 in a steady-state NO+D_2 reaction on Pd(110) at 500 K. Reproduced from data in Ref. 33. Simulated distribution forms on the plane along the [001] direction are also given. Similar 3D distributions are observed in a steady-state N_2O+D_2 (or CO) reaction or in the TPD of a NO (or N_2O)-covered surface [18]. Desorption angle θ and azimuth angle ϕ on Pd(110) are defined on the left. A top view of the Pd(110)(1×1) surface is also shown on the bottom.

Fig. 2. (a) The first observations of azimuth-angle dependence of the AR-CO_2 signal on Pd(110) under TPD conditions at low CO(a) and O(a) coverage. The desorption angle is fixed at θ=25°, and the azimuth angle (ϕ) varies. The curve is drawn to guide the eye. (b) Three-dimensional CO_2 distribution (on polar coordinates) constructed from the angular distributions along the [001] and [1$\bar{1}$0] directions. Reproduced from the data in Ref. 32. This distribution is also observed in a steady-state NO+CO reaction [33].

Fig. 3. (a) An energy-partitioning model in repulsive desorption. Arrows show repulsive forces exerted from reaction sites. A standing or lying TS is translationally excited, whereas an inclined TS torques at the desorption. (b) Flux simulations of two desorption components with $\cos^{10}(\theta)$ (hot translation) and cosine (hot rotation) forms normalized to the same total flux. A typical aperture of ±20^o for non-AR-REMPI measurements is indicated [79], whereas the non-accepted part is shadowed. (c) The respective fluxes accepted by the ±20^o aperture are given by the colored areas below the two curves (a given total flux (integrated over azimuth angles) equals the area below the respective curve over the whole [0^o,±90^o] range). It is evident that the sharper the angular distribution the larger percentage of the total flux is accepted by the ±20^o

aperture; the respective percentages of accepted flux are given in (d) for angular distributions $\cos^n(\theta)$ as a function of sharpness parameter *n*.

Fig. 4. Translational temperatures of CO_2 in CO oxidation on Pd(110) under TPD conditions vs. the desorption angle on the normally directed plane along the [001] and [1$\bar{1}$0] directions. P_1-CO_2 peaks at 420 K and P_3-CO_2 at 290 K. The latter is formed in response to higher reactant coverage yielding higher translational temperatures. Reproduced from data in Ref. 80.

Fig. 5. Rotational temperatures of CO_2 evaluated from infrared emission spectra from the desorbing product in a steady-state CO oxidation at 600 K on Pd(110)(1×1) as a function of the desorption angle along the [001] and [1$\bar{1}$0] directions. The CO pressure is higher than that of O_2 yielding a Pd(110) (1×1) form. Reproduced from data in Ref. 8.

Fig. 6. (a) Angular distributions of desorbing $^{15}N_2$ on the plane along the step-up direction (defined in Fig.10) in the catalyzed NO reduction on Pd(211) at 500 K. The steady-state $^{15}NO+D_2$ reaction was established at $P_{NO}=1.5\times10^{-5}$ Pa and $P_{D2}=2.9\times10^{-5}$ Pa. The signals observed in the direction of the increasing desorption angle (from the negative region to the positive) are designated by closed symbols and those in the decreasing desorption angle by open symbols. A typical deconvolution into $\cos^{20}(\theta+30)$ and $\cos^{1.6}(\theta+3)$ forms is indicated by broken curves. Only the former component remains below T_S=480 K; the latter becomes predominant above T_S=520 K. Solid lines indicate the summation. (b) Surface temperature dependence of angle-integrated (AI) product signals and AR $^{15}N_2$ signals at −31° off normal (the collimation angle) in a steady-state $^{15}NO+D_2$ reaction with $P_{NO}=1.5\times10^{-5}$ Pa and $P_{D2}= 1.2\times10^{-5}$ Pa. The temperature was increased stepwise to 800 K and then decreased. AR-N_2 signals observed in the direction of the increasing surface temperature are designated by filled squares and those in the downward direction by open squares. For clarity, only AI signals in the direction of increasing temperature are shown. AI-N_2: ▲; D_2O:○; N_2O:◊; ND_3:▽; and AR-$^{15}N_2$: ■, □. Reproduced from Ref.13 with permission.

Fig. 7. (a) T_S dependence of AR signals of products at the collimation positions in a steady-state $^{15}NO + D_2$ reaction on Pd(110) at $P_{NO} = 6.7\times10^{-4}$ Pa with the pressure ratio of $P_{NO}/P_{D2} = 2$. (b,c) The bottom figures show angular distributions of desorbing $^{15}N_2$ along the [001] direction at 530 K and 640 K. Typical deconvolutions indicated by broken curves are based on the velocity distribution analysis. The ordinate was normalized to the maximum at 530 K. Reproduced from Ref.114 with permission.

Fig. 8. (a) Adsorption forms of N_2O and N_2 on Pd(110) derived from DFT-GGA. The dotted circle indicates the size of a N_2 molecule estimated from van der Waals' radii. The numbers indicate the distance in nm units. (b) Proposed N_2 emission from N_2O(a)

decomposition. (i) The bent N_2O is oriented along the [001] direction. (ii) After the N–O bond cleavage, large repulsive forces (indicated by golden arrows) are induced between the nascent N_2 and the counter-product O(a). (iii) The nascent N_2 swings over the bonding metal atom and (iv) subsequently hits against the "swing wall"—an energy barrier for the substantial titling of the N_2 away from the surface normal (see Fig. 9)—due to which it finally desorbs. The N_2 fragment desorbs around the weakest N–metal bonding position.

Fig. 9. The PES of the swing motion of nascent N_2 on Pd(110), shown as the MEP for the upright-N_2 → flat-N_2 transition on Pd(110) for top- and bridge-bonded N_2; ΔE is defined as $\Delta E = E_{site} - E_{0site}$, where E_{0site} is the potential energy of the equilibrium upright N_2 adsorbed at the site, E_{site} is the energy of a given configuration at that site, and the site is either top or bridge. Adsorption bond-strengths, $|E_{ads}(site)|$, of top- and bridge-bonded N_2 are also indicated. The inset on the right of the MEPs graph shows the definition of the N−N−metal bend angles: $t_1 \equiv$ the tilt angle between N−N and Pd−N axes, $t_2 \equiv$ the tilt angle between the N−metal bond and the surface normal, and $t_c \equiv$ the angle between the surface normal and the axis linking the N_2 mass center with the adsorption site. The (t_1, t_2) angles are also stated for each point on the MEP (except the first one). Reproduced from Ref. 12 with permission. Structures corresponding to each point on the MEPs are indicated in the corresponding filmstrips.

Fig. 10. (a) Top and side views of stepped Pd(211), definition of crystal axes, and definition of the desorption angle, θ. The step-up direction is perpendicular to step-edge along the positive θ angles (and vice-versa for the step-down direction). Adsorption structures of the N_2O intermediate as predicted by DFT calculations: (b) the most stable adsorption form, (c) adsorption form on the (111) terrace, (d) transition state structure for NN−O dissociation, and (e) the swing motion of product N_2 after the N−O bond cleavage, followed by desorption. Adopted from from Ref. 12 with permission.

Fig. 11. MEP for the upright-N_2 → flat-N_2 transition along the $[1\bar{1}\bar{1}]$ direction on Pd(211). Each point on the MEP corresponds to a respective structure shown on the filmstrip. Note that the flat-N_2 (last structure) does not correspond to a local minimum on the PES but was constrained to the bridge position (actually the axis of N_2 was constrained in the $[1\bar{1}\bar{1}]$ direction for the whole MEP); if this constraint is lifted, then the N_2 relaxes by displacing the N atom at the step-edge bridge site to a step-edge top site. The inset shows the definition of the N−N−metal bend angle t_1 and the tilt angle t_2 between the N−metal bond and the local (111) surface normal. For all but the first point on the MEP, the (t_1, t_2) angles are also stated. ΔE is defined analogously as in Fig. 9. The horizontal blue dashed line indicates the desorption energy (E_{des}) of the upright N_2. Reproduced from Ref. 12 with permission.

Fig. 12. Spatial distributions (on polar coordinates) of desorbing N_2 in TPD procedures of N_2O-covered Rh(100). The desorption peak (β_2-N_2) appears at around 85 K. The initial coverages are also given. Reproduced from Ref. 146 with permission.

Fig. 13. Mean translational energy of D_2 versus rotational energy on Cu(111). The mean translational energy determined from the non-AR-REMPI-TOF at each rotational state and different vibrational states is plotted against the rotational energy estimated from quantum number J. The solid blue line shows only a slope expected from the EP model (no meaning in the absolute values). Reproduced from the data in Ref. 79 (open symbols) and Ref. 166 (closed symbols). The position of J=5 is indicated by the vertical dashed-dotted line.

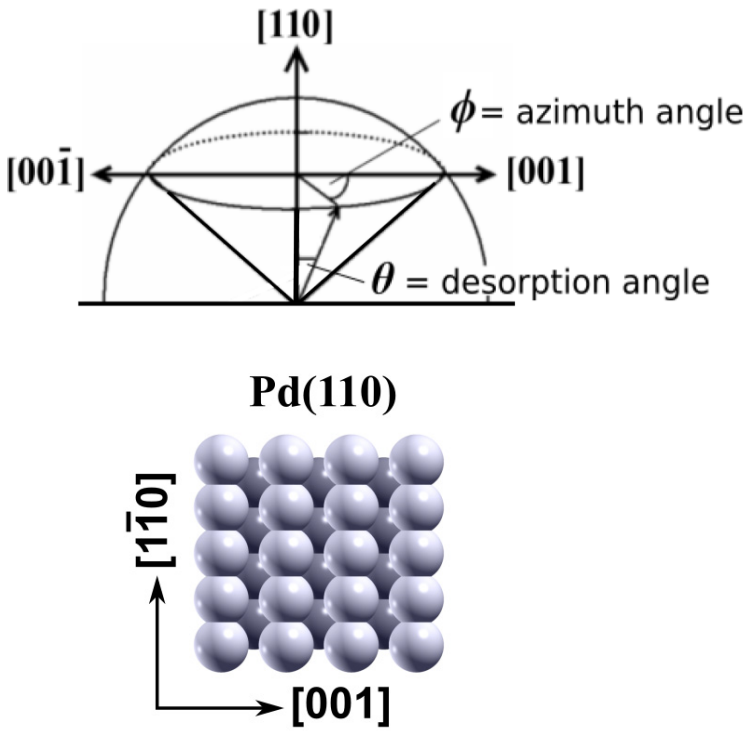

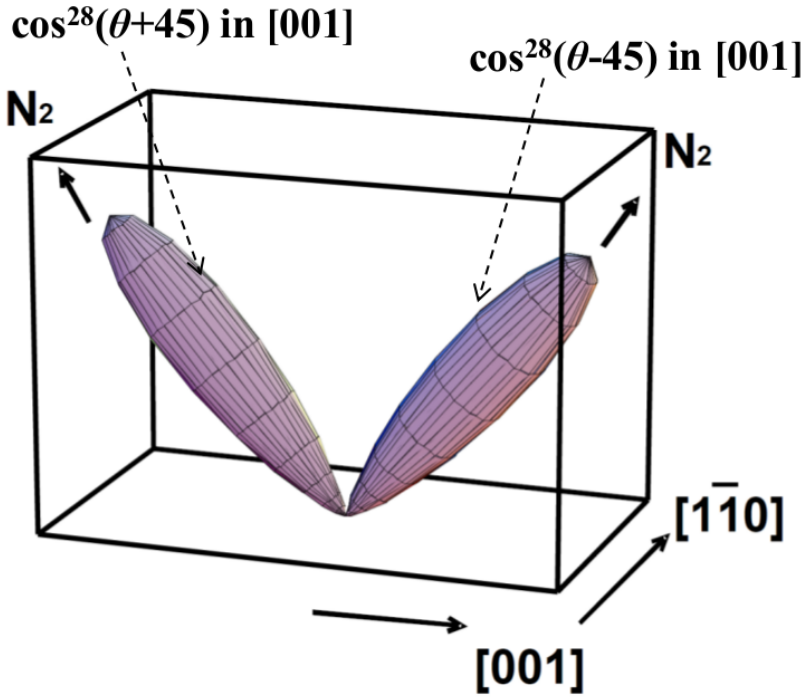

$N_2O(a) \rightarrow N_2(g)+O(a)$

Fig.1

(a)

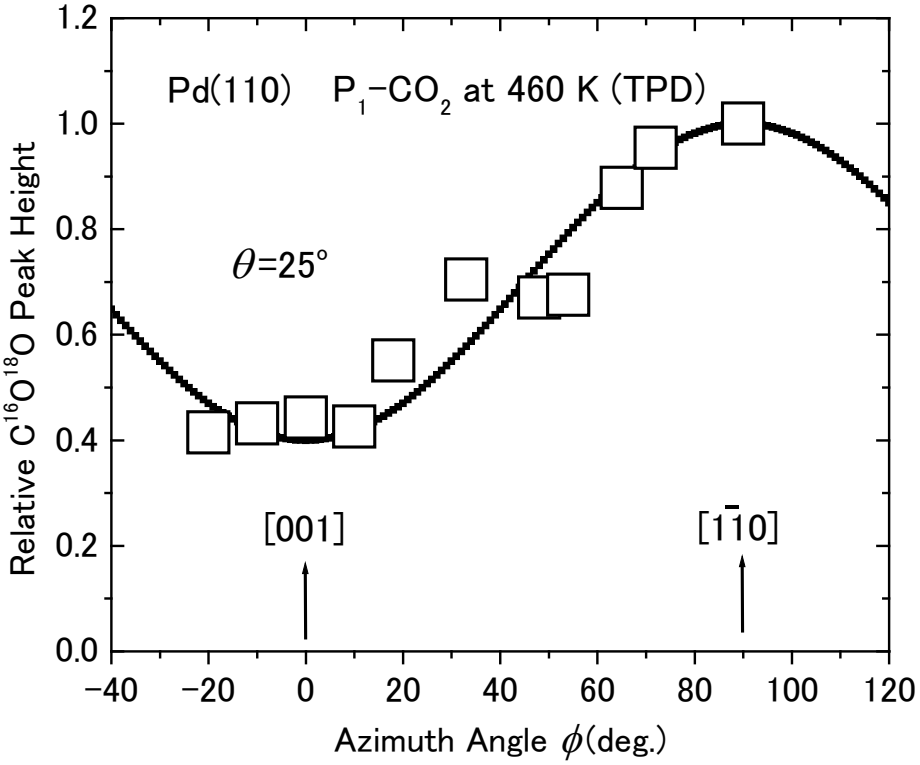

$$CO(a)+O(a) \rightarrow CO_2(g)$$

(b)

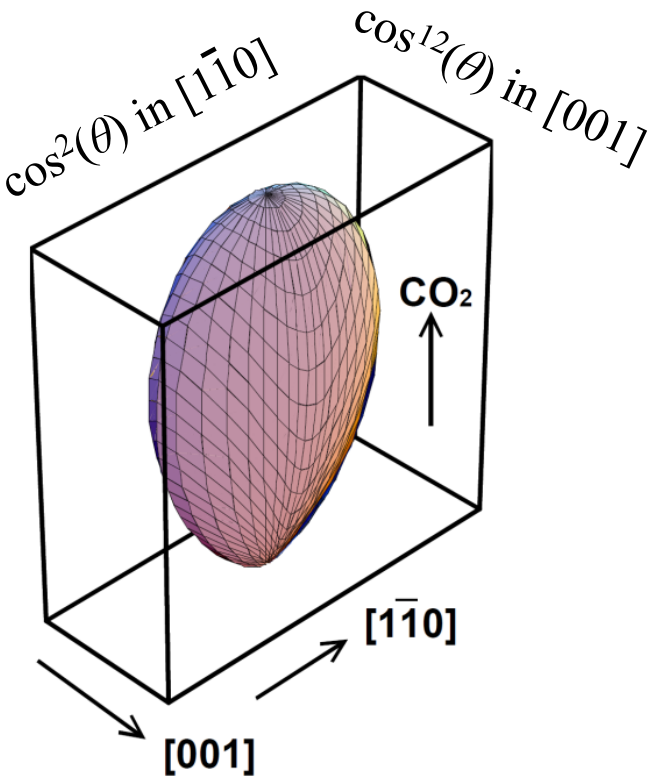

Fig.2

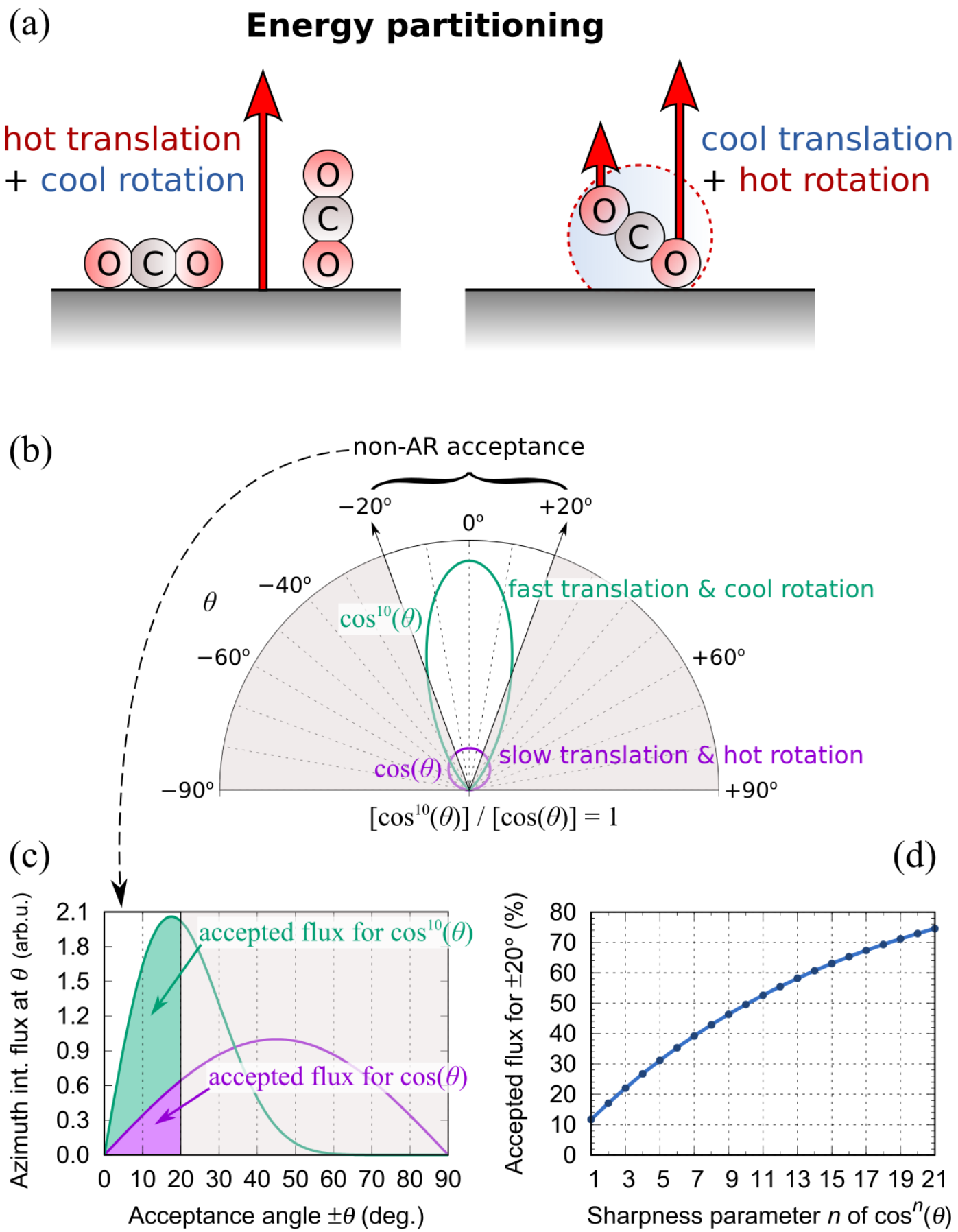
(a)
Energy partitioning
hot translation
+ cool rotation
O C O
O C O
cool translation
+ hot rotation
O C O
(b)
non-AR acceptance
−20°
+20°
0°
−40°
θ
fast translation & cool rotation
cos10(θ)
−60°
+60°
slow translation & hot rotation
cos(θ)
−90°
+90°
[cos10(θ)] / [cos(θ)] = 1
(c)
(d)
Azimuth int. flux at θ (arb.u.)
2.1
1.8
1.5
1.2
0.9
0.6
0.3
0.0
accepted flux for cos10(θ)
accepted flux for cos(θ)
0 10 20 30 40 50 60 70 80 90
Acceptance angle ±θ (deg.)
Accepted flux for ±20° (%)
80
70
60
50
40
30
20
10
0
1 3 5 7 9 11 13 15 17 19 21
Sharpness parameter n of cosn(θ)

Fig.3

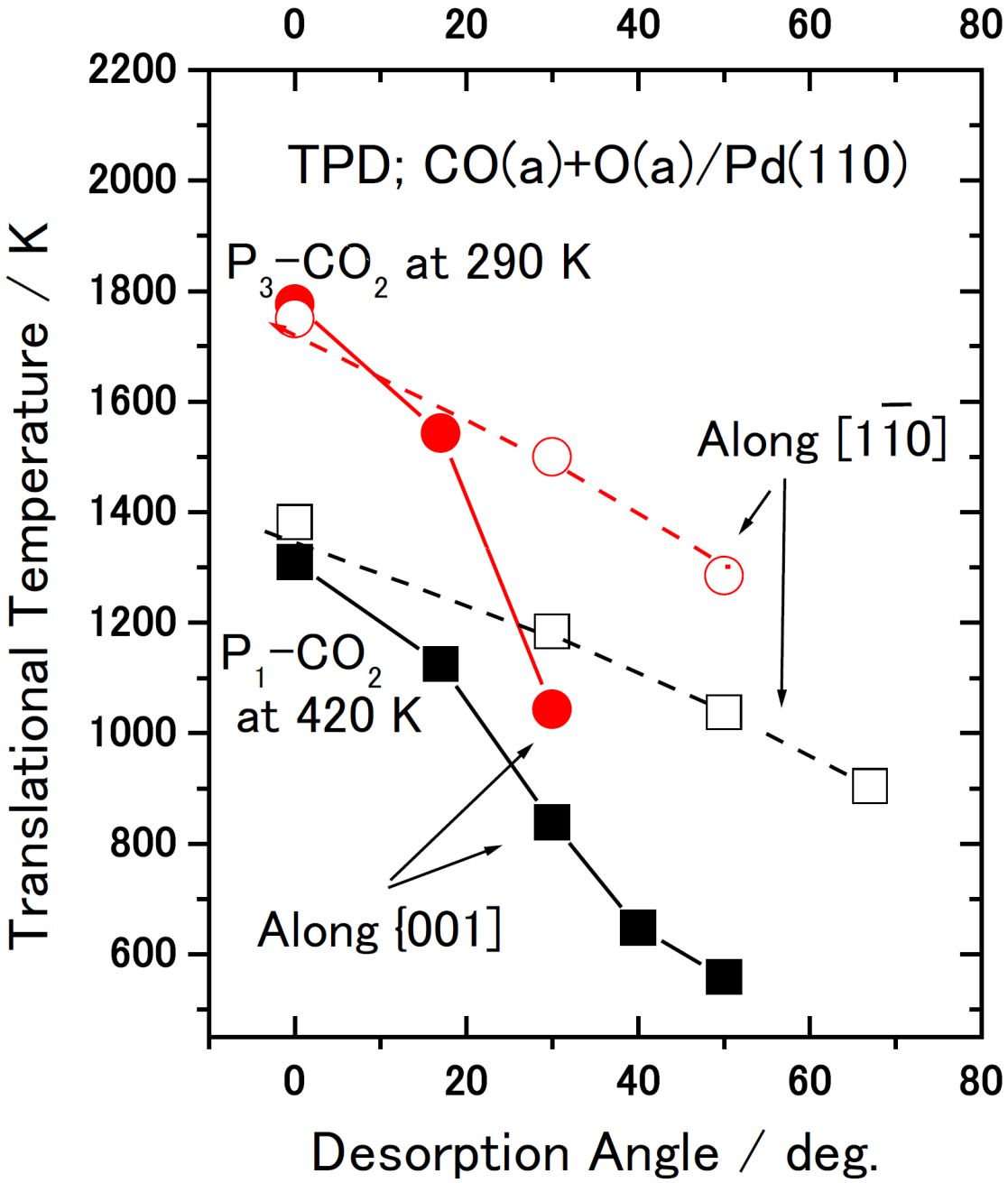
TPD; CO(a)+O(a)/Pd(110)
P3–CO2 at 290 K
P1–CO2 at 420 K
Along [1$\bar{1}$0]
Along {001]
Translational Temperature / K
Desorption Angle / deg.
0
20
40
60
80
2200
2000
1800
1600
1400
1200
1000
800
600

Fig 4

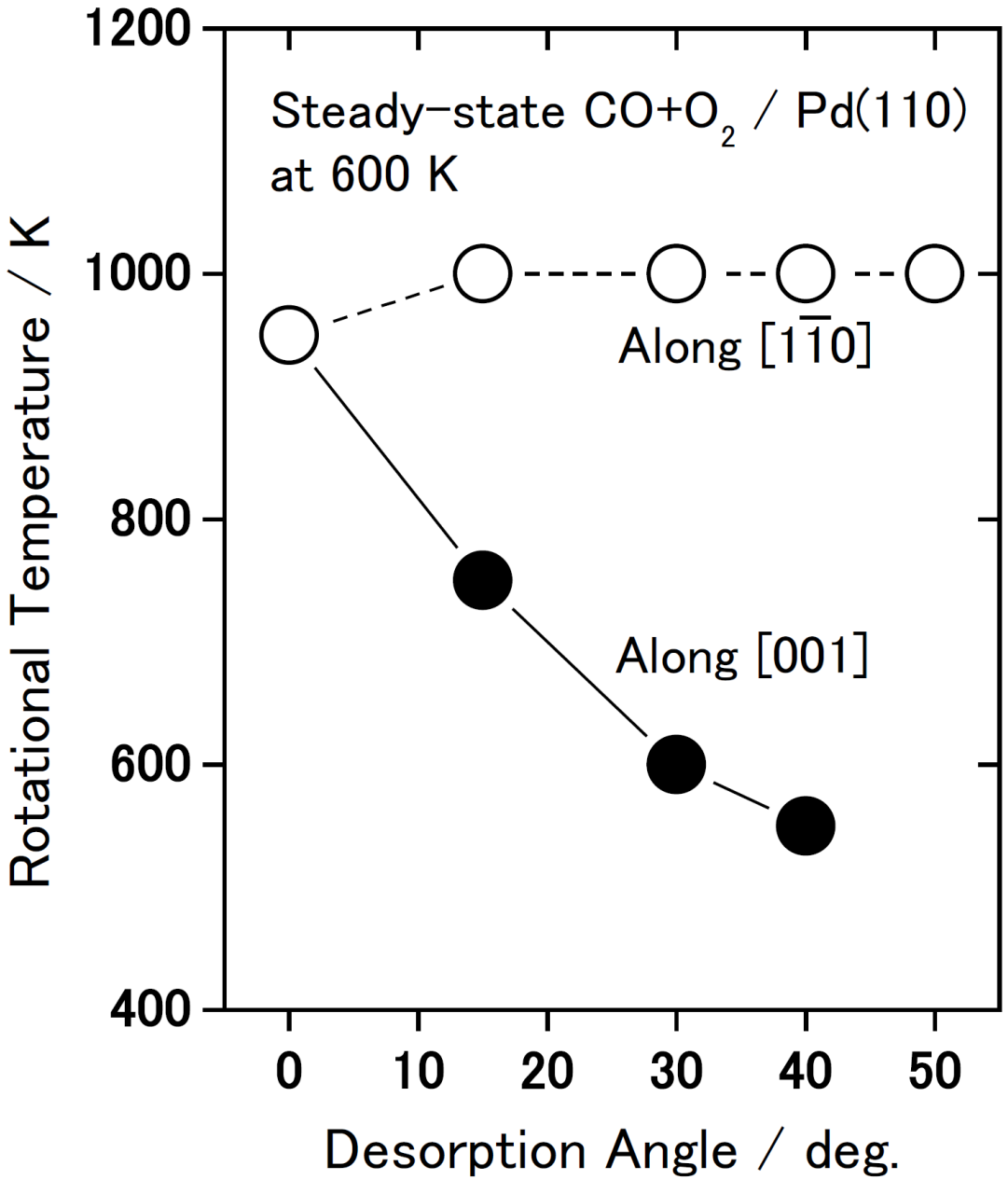
Steady-state CO+O2 / Pd(110)
at 600 K
Along [1$\bar{1}$0]
Along [001]
Rotational Temperature / K
Desorption Angle / deg.
1200
1000
800
600
400
0
10
20
30
40
50

Fig.5

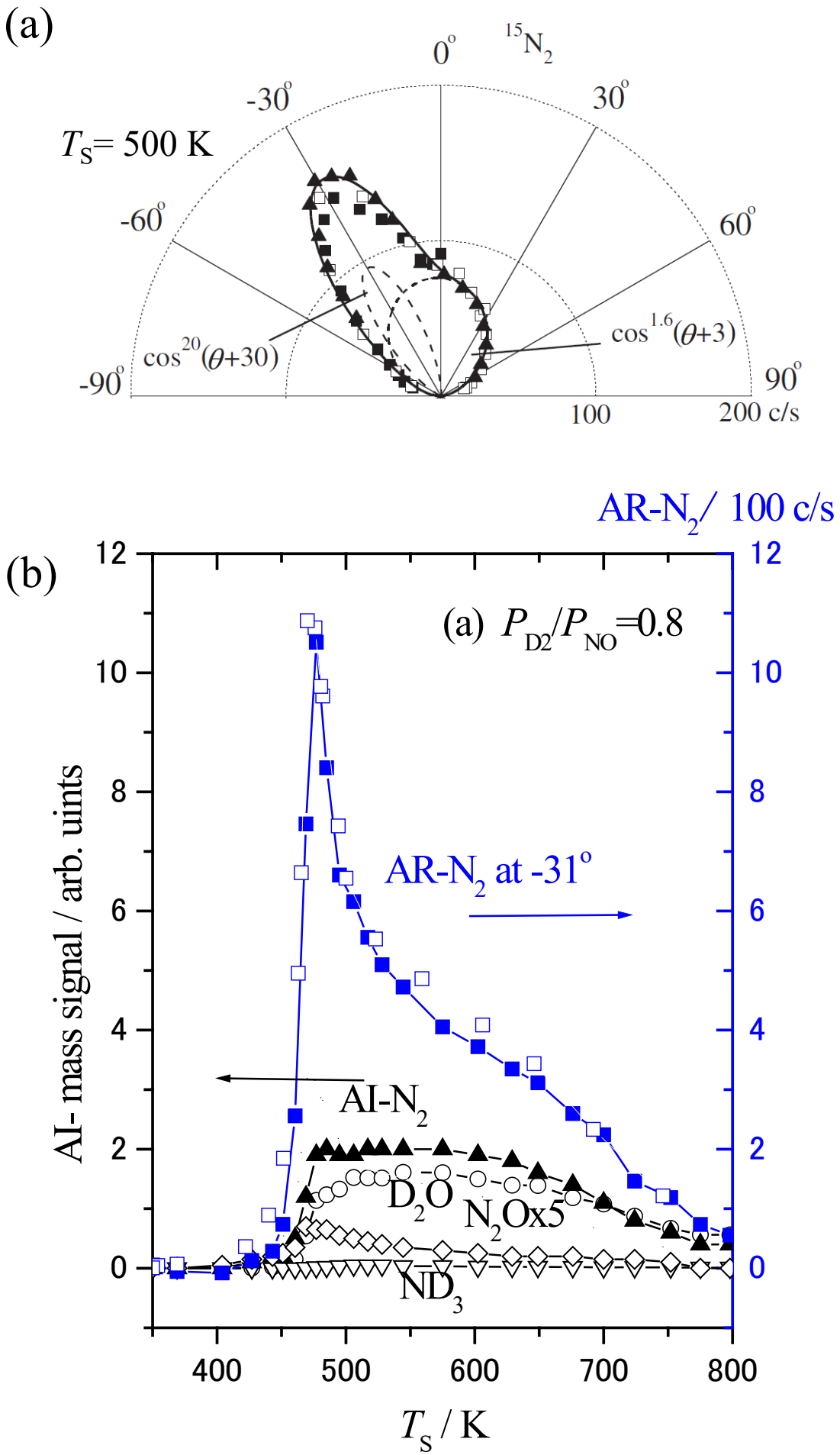
(a)
T_S= 500 K
0°
$^{15}N_2$
-30°
30°
-60°
60°
-90°
90°
cos^{20}(θ+30)
cos$^{1.6}$(θ+3)
100
200 c/s
(b)
(a) P_{D2}/P_{NO}=0.8
AR-N$_2$/ 100 c/s
AR-N$_2$ at -31°
AI-N$_2$
D$_2$O
N$_2$Ox5
ND$_3$
AI- mass signal / arb. uints
T_S / K
0
2
4
6
8
10
12
400
500
600
700
800

Fig.6

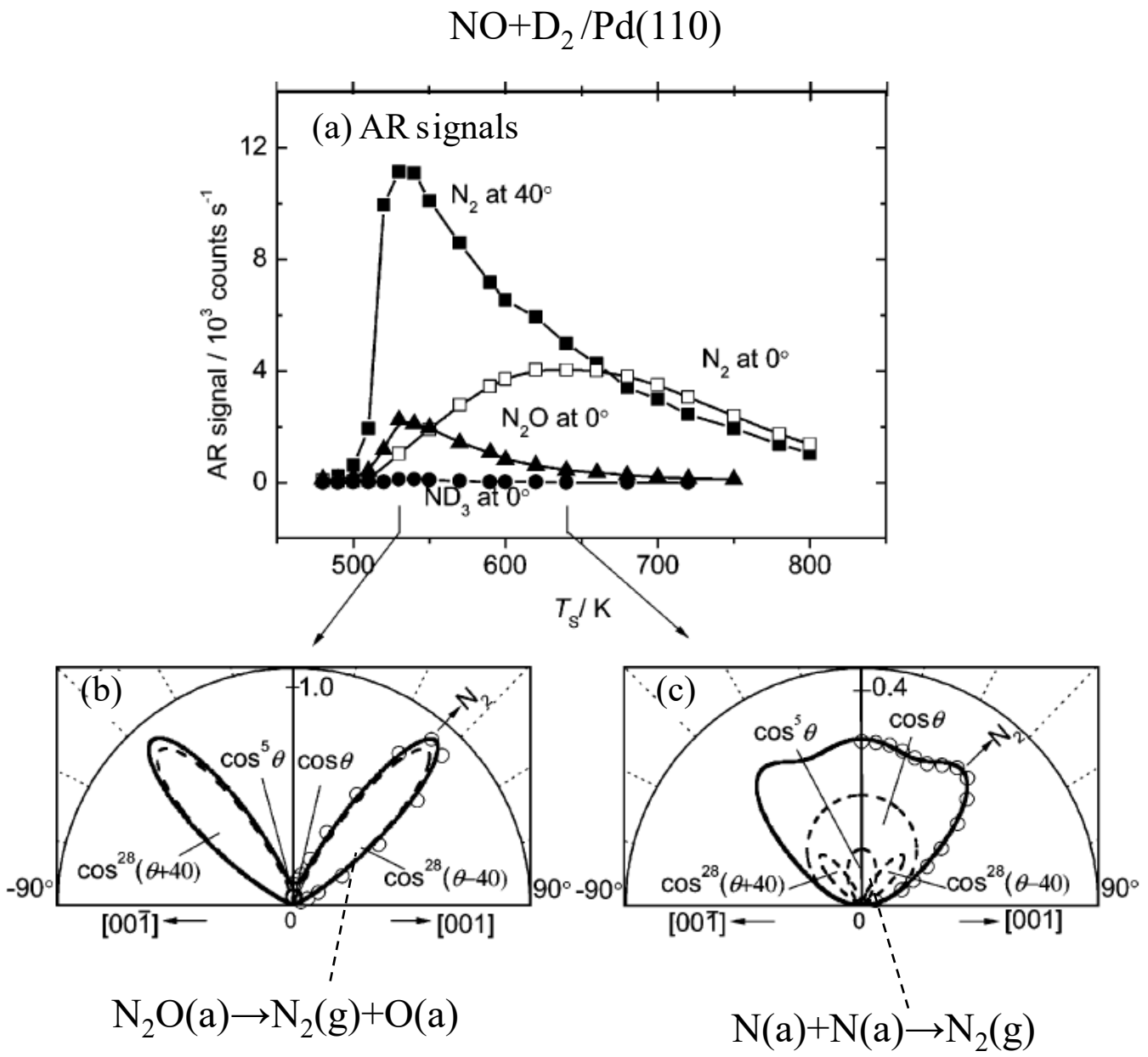
NO+D2 /Pd(110)
(a) AR signals
AR signal / 10^3 counts s^-1
N2 at 40°
N2 at 0°
N2O at 0°
ND3 at 0°
Ts / K
(b)
1.0
N2
cos^5 θ
cos θ
cos^28(θ+40)
cos^28(θ−40)
-90°
90°
[00$\bar{1}$]
0
[001]
(c)
0.4
N2
cos^5 θ
cos θ
cos^28(θ+40)
cos^28(θ−40)
-90°
90°
[00$\bar{1}$]
0
[001]
N2O(a)→N2(g)+O(a)
N(a)+N(a)→N2(g)

Fig. 7

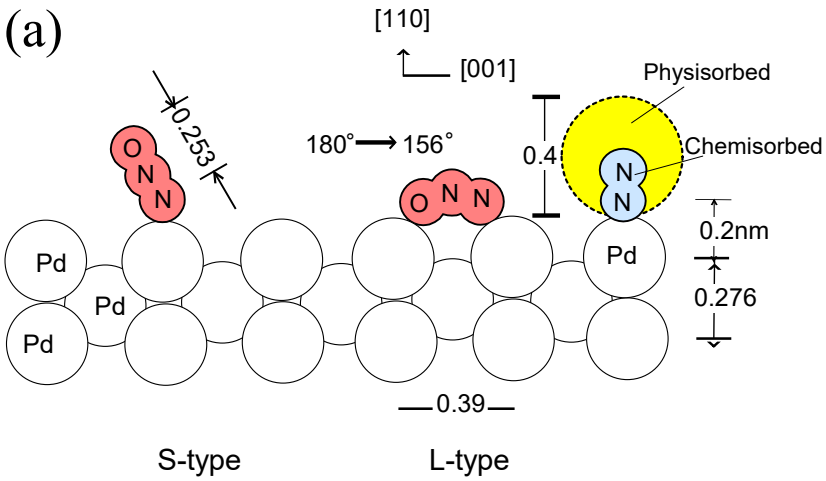
(a)
[110]
[001]
Physisorbed
Chemisorbed
0.253
180° → 156°
0.4
O N N
N N
Pd
Pd
Pd
Pd
0.2nm
0.276
0.39
S-type
L-type

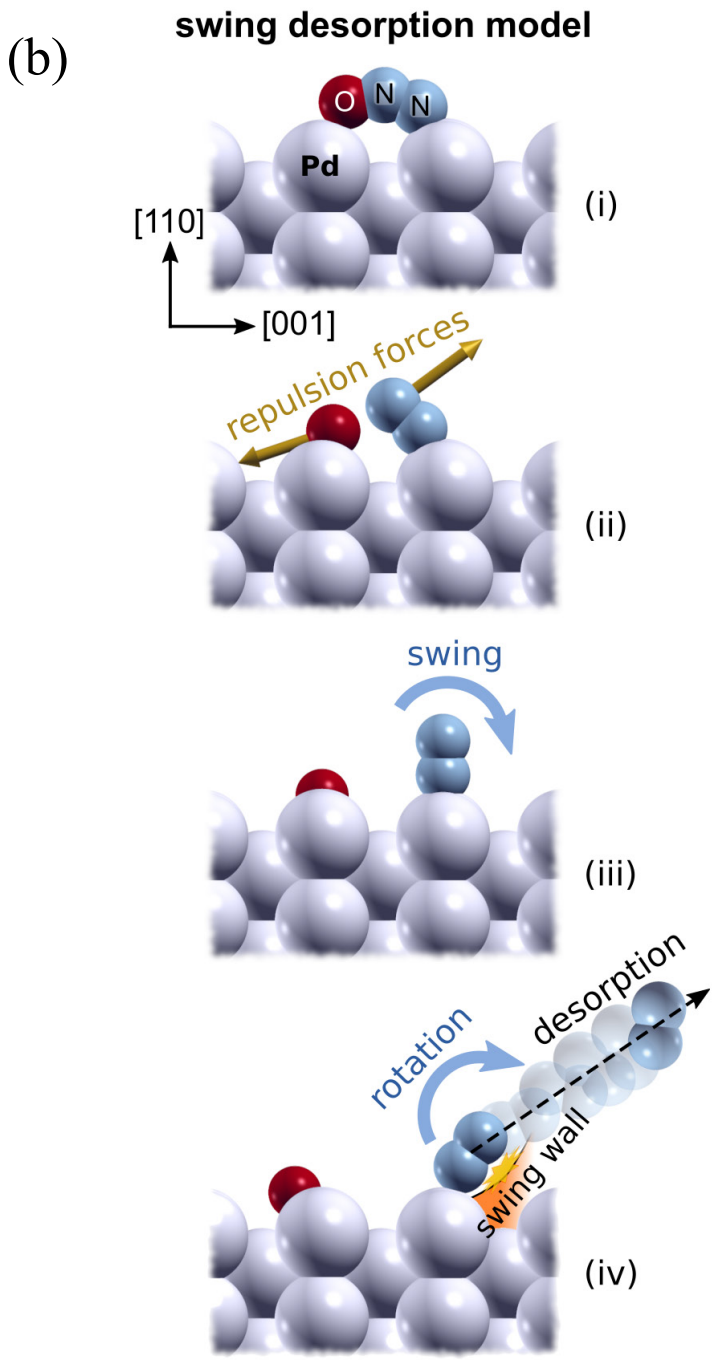
(b)
swing desorption model
O N N
Pd
[110]
[001]
(i)
repulsion forces
(ii)
swing
(iii)
rotation
desorption
swing wall
(iv)

Fig.8

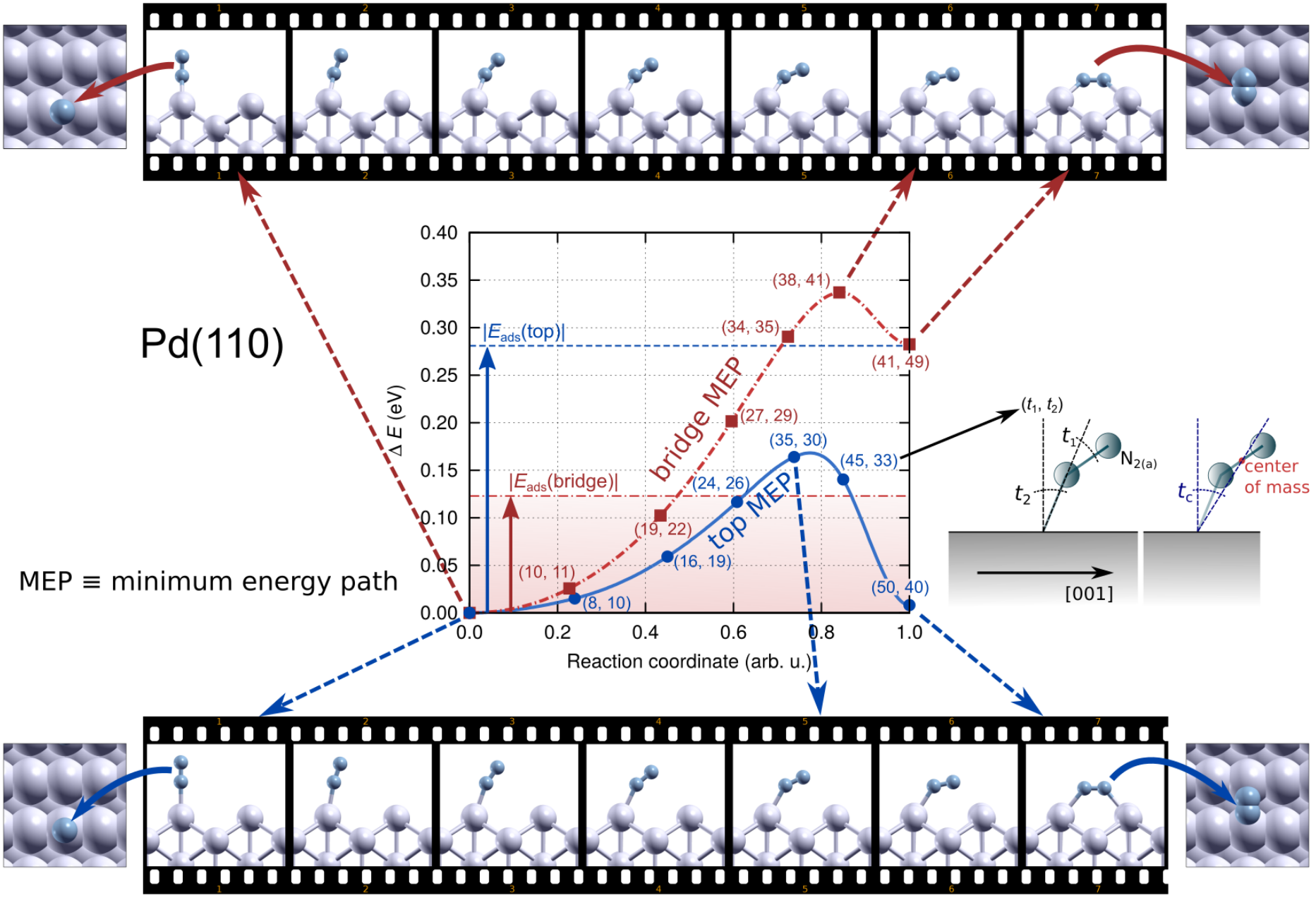
Pd(110)
MEP ≡ minimum energy path
Δ E (eV)
Reaction coordinate (arb. u.)
|E_ads(top)|
|E_ads(bridge)|
bridge MEP
top MEP
(38, 41)
(34, 35)
(41, 49)
(27, 29)
(35, 30)
(45, 33)
(24, 26)
(19, 22)
(16, 19)
(10, 11)
(8, 10)
(50, 40)
(t1, t2)
t1
t2
N2(a)
tc
center of mass
[001]

Fig.9

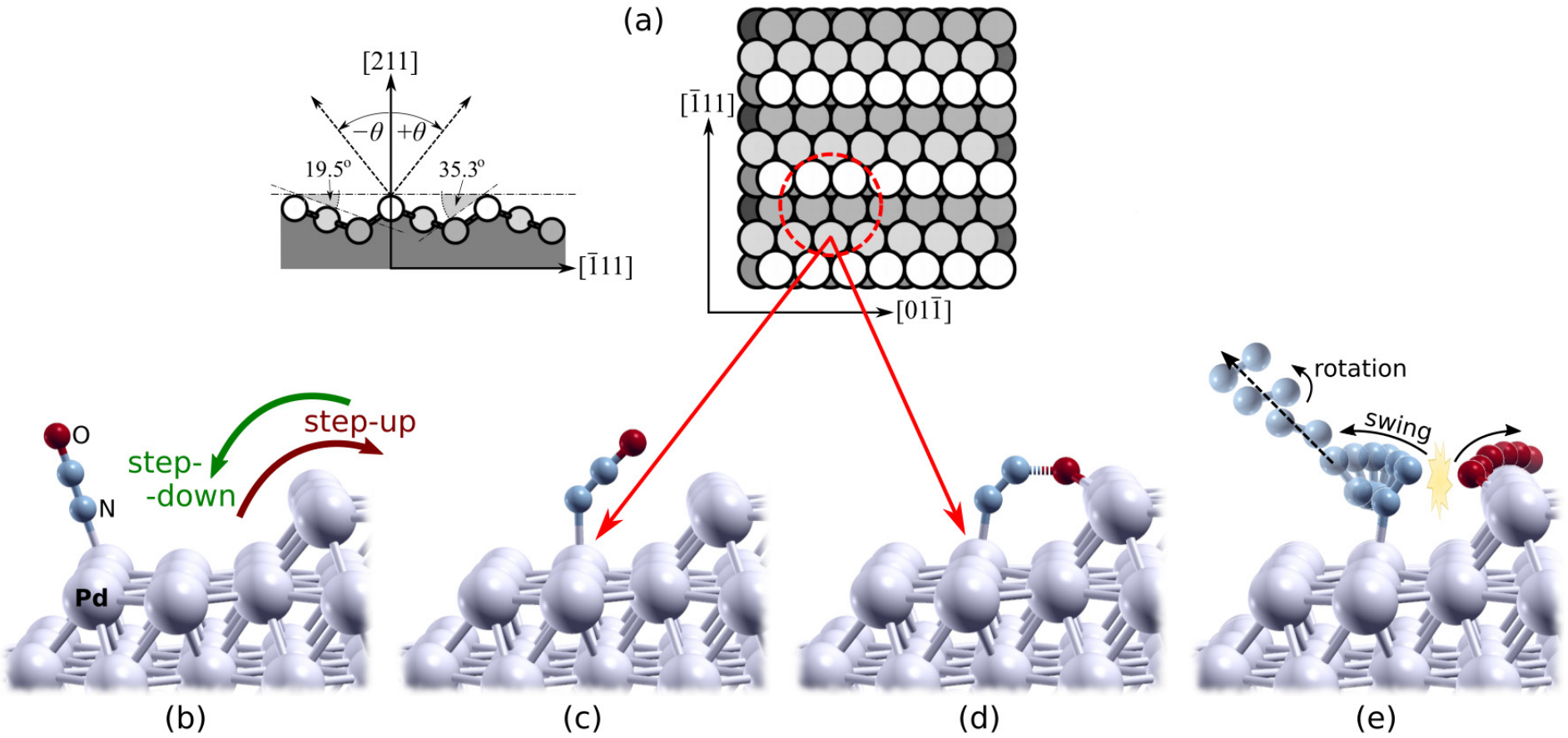
(a)
[211]
−θ
+θ
19.5°
35.3°
[$\bar{1}$11]
[$\bar{1}$11]
[01$\bar{1}$]
step-up
step-
-down
O
N
Pd
rotation
swing
(b)
(c)
(d)
(e)

Fig.10

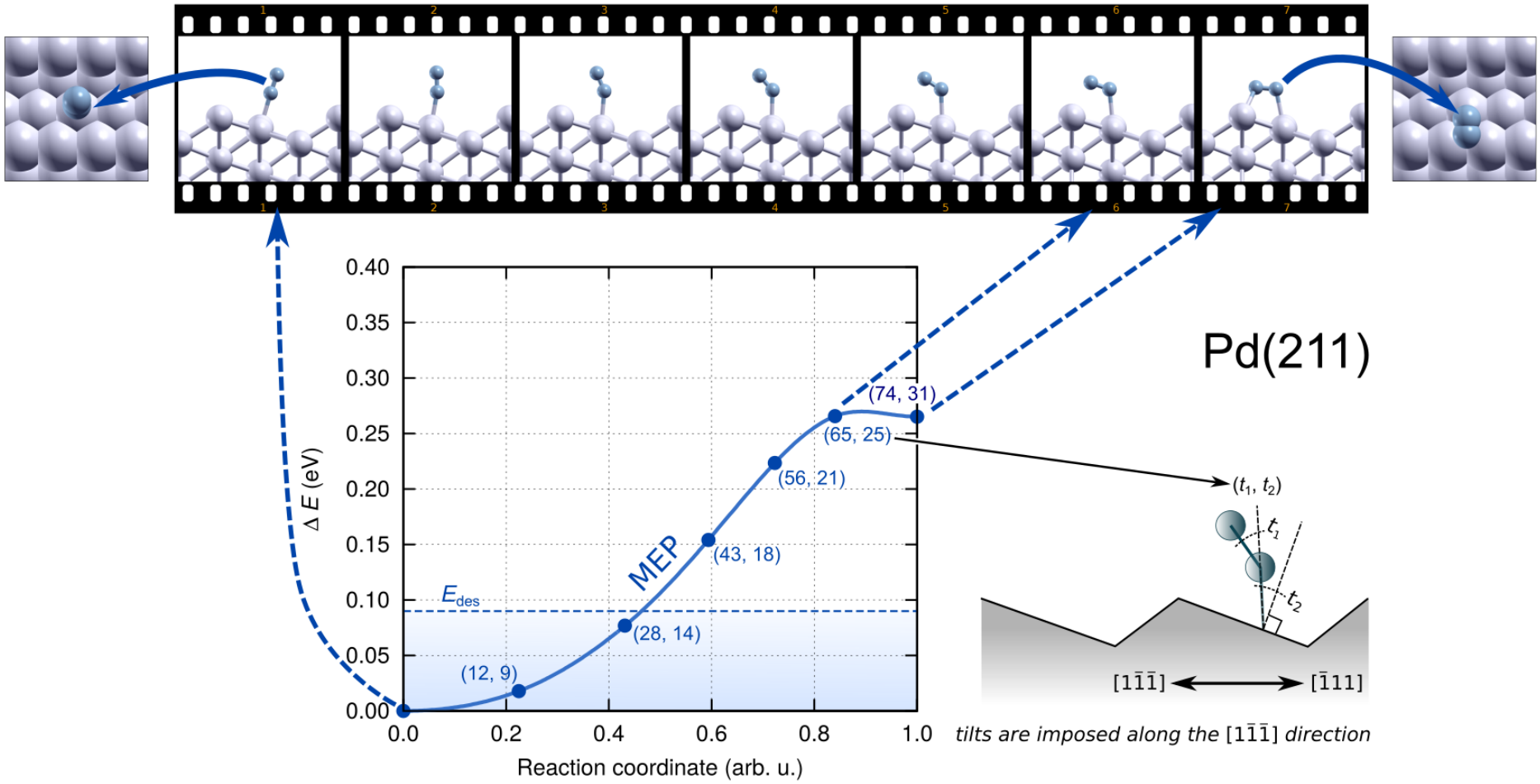
Pd(211)
MEP
E_{des}
(12, 9)
(28, 14)
(43, 18)
(56, 21)
(65, 25)
(74, 31)
ΔE (eV)
Reaction coordinate (arb. u.)
0.00
0.05
0.10
0.15
0.20
0.25
0.30
0.35
0.40
0.0
0.2
0.4
0.6
0.8
1.0
(t_1, t_2)
t_1
t_2
$[1\bar{1}\bar{1}]$
$[\bar{1}11]$
tilts are imposed along the $[1\bar{1}\bar{1}]$ *direction*

Fig.11

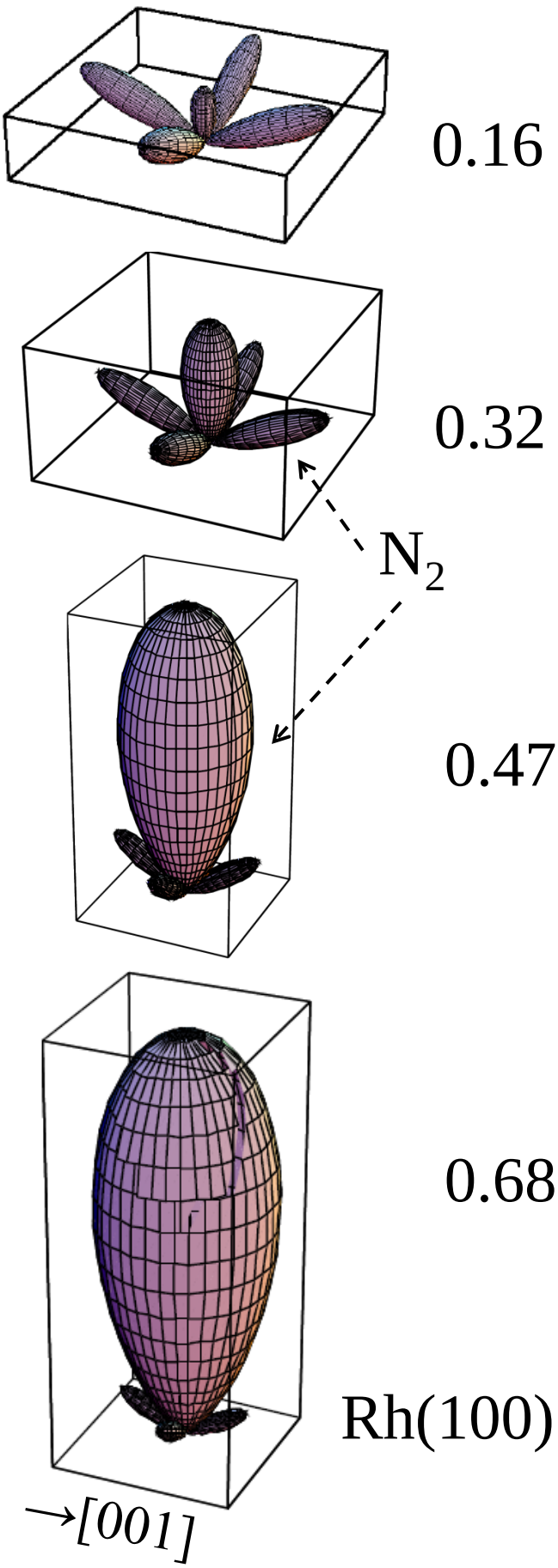

Fig.12

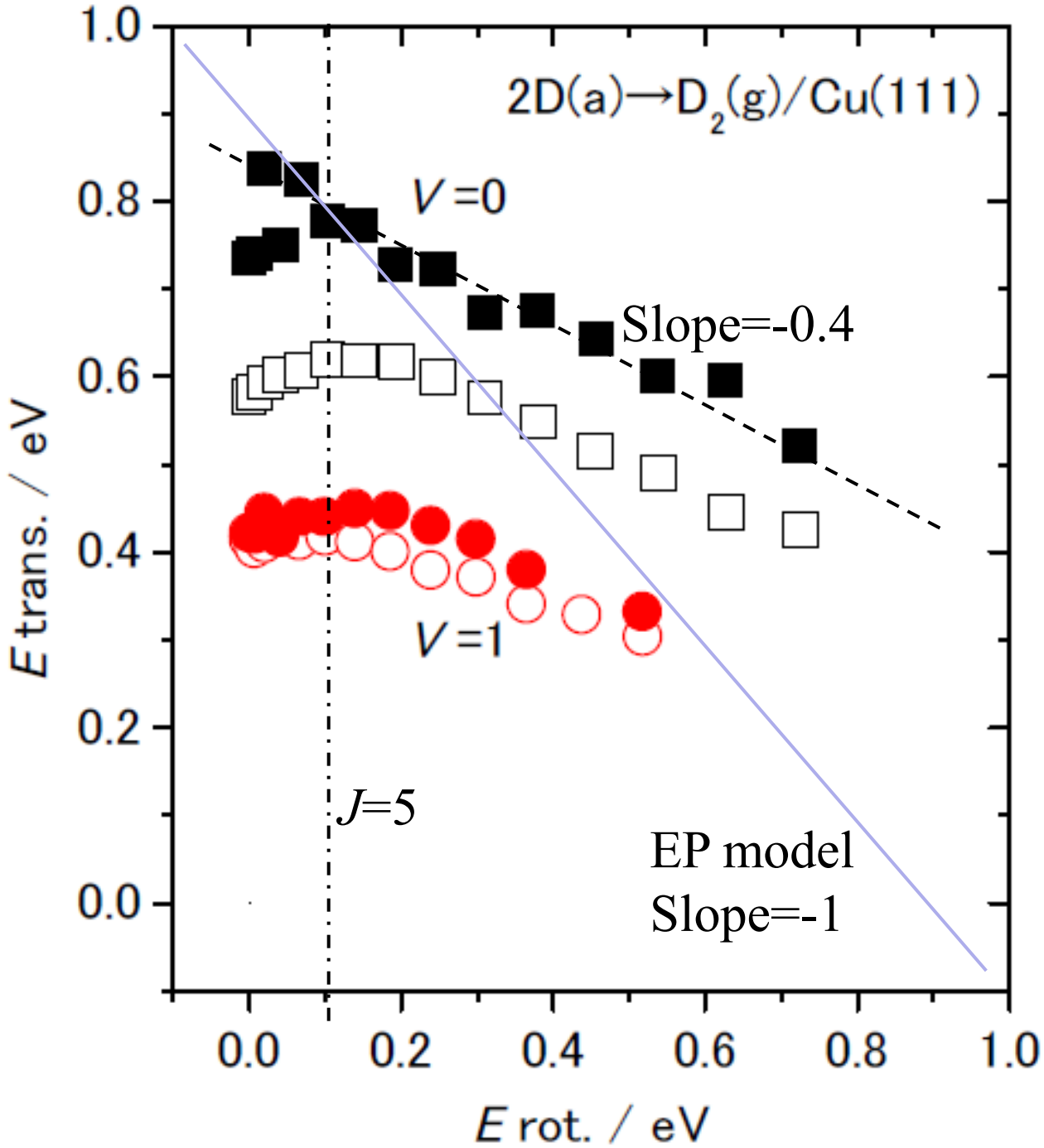
2D(a)→D2(g)/Cu(111)
V=0
Slope=-0.4
V=1
J=5
EP model
Slope=-1
E trans. / eV
E rot. / eV
1.0
0.8
0.6
0.4
0.2
0.0
0.0
0.2
0.4
0.6
0.8
1.0

Fig. 13